

International Journal of Physical Sciences

Volume 9 Number 16 30 August, 2014

ISSN 1992-1950



*Academic
Journals*

ABOUT IJPS

The **International Journal of Physical Sciences (IJPS)** is published weekly (one volume per year) by Academic Journals.

International Journal of Physical Sciences (IJPS) is an open access journal that publishes high-quality solicited and unsolicited articles, in English, in all Physics and chemistry including artificial intelligence, neural processing, nuclear and particle physics, geophysics, physics in medicine and biology, plasma physics, semiconductor science and technology, wireless and optical communications, materials science, energy and fuels, environmental science and technology, combinatorial chemistry, natural products, molecular therapeutics, geochemistry, cement and concrete research, metallurgy, crystallography and computer-aided materials design. All articles published in IJPS are peer-reviewed.

Contact Us

Editorial Office: ijps@academicjournals.org

Help Desk: helpdesk@academicjournals.org

Website: <http://www.academicjournals.org/journal/IJPS>

Submit manuscript online <http://ms.academicjournals.me/>

Editors

Prof. Sanjay Misra

*Department of Computer Engineering, School of Information and Communication Technology
Federal University of Technology, Minna,
Nigeria.*

Prof. Songjun Li

*School of Materials Science and Engineering,
Jiangsu University,
Zhenjiang,
China*

Dr. G. Suresh Kumar

*Senior Scientist and Head Biophysical Chemistry
Division Indian Institute of Chemical Biology
(IICB)(CSIR, Govt. of India),
Kolkata 700 032,
INDIA.*

Dr. Remi Adewumi Oluyinka

*Senior Lecturer,
School of Computer Science
Westville Campus
University of KwaZulu-Natal
Private Bag X54001
Durban 4000
South Africa.*

Prof. Hyo Choi

*Graduate School
Gangneung-Wonju National University
Gangneung,
Gangwondo 210-702, Korea*

Prof. Kui Yu Zhang

*Laboratoire de Microscopies et d'Etude de
Nanostructures (LMEN)
Département de Physique, Université de Reims,
B.P. 1039. 51687,
Reims cedex,
France.*

Prof. R. Vittal

*Research Professor,
Department of Chemistry and Molecular
Engineering
Korea University, Seoul 136-701,
Korea.*

Prof Mohamed Bououdina

*Director of the Nanotechnology Centre
University of Bahrain
PO Box 32038,
Kingdom of Bahrain*

Prof. Geoffrey Mitchell

*School of Mathematics,
Meteorology and Physics
Centre for Advanced Microscopy
University of Reading Whiteknights,
Reading RG6 6AF
United Kingdom.*

Prof. Xiao-Li Yang

*School of Civil Engineering,
Central South University,
Hunan 410075,
China*

Dr. Sushil Kumar

*Geophysics Group,
Wadia Institute of Himalayan Geology,
P.B. No. 74 Dehra Dun - 248001(UC)
India.*

Prof. Suleyman KORKUT

*Duzce University
Faculty of Forestry
Department of Forest Industrial Engineering
Beciyorukler Campus 81620
Duzce-Turkey*

Prof. Nazmul Islam

*Department of Basic Sciences &
Humanities/Chemistry,
Techno Global-Balurghat, Mangalpur, Near District
Jail P.O: Beltalapak, P.S: Balurghat, Dist.: South
Dinajpur,
Pin: 733103,India.*

Prof. Dr. Ismail Musirin

*Centre for Electrical Power Engineering Studies
(CEPES), Faculty of Electrical Engineering, Universiti
Teknologi Mara,
40450 Shah Alam,
Selangor, Malaysia*

Prof. Mohamed A. Amr

*Nuclear Physic Department, Atomic Energy Authority
Cairo 13759,
Egypt.*

Dr. Armin Shams

*Artificial Intelligence Group,
Computer Science Department,
The University of Manchester.*

Editorial Board

Prof. Salah M. El-Sayed

*Mathematics. Department of Scientific Computing,
Faculty of Computers and Informatics,
Benha University. Benha ,
Egypt.*

Dr. Rowdra Ghatak

*Associate Professor
Electronics and Communication Engineering Dept.,
National Institute of Technology Durgapur
Durgapur West Bengal*

Prof. Fong-Gong Wu

*College of Planning and Design, National Cheng Kung
University
Taiwan*

Dr. Abha Mishra.

*Senior Research Specialist & Affiliated Faculty.
Thailand*

Dr. Madad Khan

*Head
Department of Mathematics
COMSATS University of Science and Technology
Abbottabad, Pakistan*

Prof. Yuan-Shyi Peter Chiu

*Department of Industrial Engineering & Management
Chaoyang University of Technology
Taichung, Taiwan*

Dr. M. R. Pahlavani,

*Head, Department of Nuclear physics,
Mazandaran University,
Babolsar-Iran*

Dr. Subir Das,

*Department of Applied Mathematics,
Institute of Technology, Banaras Hindu University,
Varanasi*

Dr. Anna Oleksy

*Department of Chemistry
University of Gothenburg
Gothenburg,
Sweden*

Prof. Gin-Rong Liu,

*Center for Space and Remote Sensing Research
National Central University, Chung-Li,
Taiwan 32001*

Prof. Mohammed H. T. Qari

*Department of Structural geology and remote sensing
Faculty of Earth Sciences
King Abdulaziz UniversityJeddah,
Saudi Arabia*

Dr. Jyhwen Wang,

*Department of Engineering Technology and Industrial
Distribution
Department of Mechanical Engineering
Texas A&M University
College Station,*

Prof. N. V. Sastry

*Department of Chemistry
Sardar Patel University
Vallabh Vidyanagar
Gujarat, India*

Dr. Edilson Ferneda

*Graduate Program on Knowledge Management and IT,
Catholic University of Brasilia,
Brazil*

Dr. F. H. Chang

*Department of Leisure, Recreation and Tourism
Management,
Tzu Hui Institute of Technology, Pingtung 926,
Taiwan (R.O.C.)*

Prof. Annapurna P.Patil,

*Department of Computer Science and Engineering,
M.S. Ramaiah Institute of Technology, Bangalore-54,
India.*

Dr. Ricardo Martinho

*Department of Informatics Engineering, School of
Technology and Management, Polytechnic Institute of
Leiria, Rua General Norton de Matos, Apartado 4133, 2411-
901 Leiria,
Portugal.*

Dr Driss Miloud

*University of mascara / Algeria
Laboratory of Sciences and Technology of Water
Faculty of Sciences and the Technology
Department of Science and Technology
Algeria*

ARTICLES

- Study of miscibility of liquid mixtures with a critical point:
A new experiment for a physical chemistry course** **350**
Filomena Califano, Guram Nozadze, Alexander Ly van Manh and Ahmed Farhat
- Electrical properties and crystal structure of Y123, Y358 and Y257/Y211
composite bulk superconductors** **360**
Kruaehong T.
- Effect of an axial magnetic field on the heat and mass transfer
in rotating annulus** **368**
Sofiane ABERKANE, Malika IHDENE, Mourad MODERES and Abderahmane GHEZAL

Full Length Research Paper

Study of miscibility of liquid mixtures with a critical point: A new experiment for a physical chemistry course

Filomena Califano*, Guram Nozadze, Alexander Ly van Manh and Ahmed Farhat

Department of Chemistry and Physics, St. Francis College, USA.

Received 10 June, 2013; Accepted 5 February, 2014

This paper describes a new experiment for undergraduate students in physical chemistry. This experiment describes a separation process of liquid-liquid extraction using mixtures with a critical point of miscibility. In this experiment, students will learn how to measure solute concentration, and a new liquid-liquid extraction technique that we called Phase Transition Extraction (PTE). In this experiment, a liquid mixture, together with the solute to be separated, is first heated above its critical temperature, where it forms a uniform solution, and then cooled to the region below the miscibility curve, where it separates. Students will understand that this separation process has the advantage that the resulting separation of the solvents is very rapid. In addition, the extraction speed of it may be 10 times higher than that of the traditional liquid-liquid extraction. The new process is thought of having significant advantages in the extraction of products from fermentation broths, plants, and other natural sources. In this paper, miscibility of binary liquid mixtures of methanol-cyclohexane and acetonitrile-water-toluene will be studied. A two-phase distribution ratio will be determined. Temperature and composition of the liquid-liquid critical point will be determined.

Key words: Miscibility, liquid mixtures, methanol-cyclohexane, acetonitrile-water-toluene.

INTRODUCTION

Liquid-liquid extraction process

Liquid-liquid extraction (LLE) has important uses in many industries and has been extensively studied (Treybal, 1963; Hanson, 1971; Lo et al., 1983; Alegert, 1988). Such processes are used both for the extraction of one compound as well as for the separation between two or more compounds (fractional extraction). In one sense there is a strong similarity between the distillation and the LLE processes. In both cases the operations generally

rely upon the unequal equilibrium distribution of substances to be separated between two phases. However, while in the distillation operation the two phases are generated from the original solution by addition of heat, and the components of the original solution then distribute unequally between the liquid and vapor phases; in the LLE process, the second phase is created by addition of extraction solvent, and the solutes are distributed between two liquid phases.

In general, LLE will be preferred either where distillation

*Corresponding author. E-mail: califano_filomena@yahoo.com

Author(s) agree that this article remain permanently open access under the terms of the [Creative Commons Attribution License 4.0 International License](https://creativecommons.org/licenses/by/4.0/)

fails or where, despite some disadvantages, it provides a less expensive overall process than the distillation process. The following list indicates some typical examples where LLE has demonstrated its unique abilities as a separation method.

a) As a substitute for distillation process where LLE is less expensive.

i) Separation of liquids whose boiling point is very close. An example is the separation of butadiene (b.p. - 4.75°C) from Butylenes (b.p. - 6°C).

ii) Separation of liquids of poor relative volatility. An example is the separation of acetic acid and water, which, despite their relatively large difference in boiling point, have poor relative volatility.

iii) For mixtures with very high boiling point where high vacuum is essential for the distillation process, like long-chain fatty acids and vitamins.

b) As separation means where distillation fails.

i) Separation of heat-sensitive substances such as antibiotics.

ii) Separation of solvents that form azeotropes.

iii) Separation according to chemical type, where boiling points overlap. An example is the separation of aromatic hydrocarbons from paraffin hydrocarbons.

The LLE process procedure is simple in concept and usually requires contacting of feed containing the solute to be extracted with a solvent, this solvent/feed mixture is usually immiscible but may be partially miscible in some cases.

After forward extraction, the solute remains in the solvent phase and depleted feed becomes the raffinate. In fractional extraction, the extract is scrubbed with an immiscible phase (usually involving the same phase type as the original feed) in order to improve the purity of final product. After scrubbing, the solvent is stripped of its solute and the regenerated solvent returned as solvent feed to the process. Often the returned solvent is washed to remove breakdown products. The strip solution provides a product stream.

It is important at this stage to recognize certain features of the process that the present work will seek to change. The extraction and the stripping involve liquid-liquid contact in which the droplets of one phase are dispersed in a second phase and mass-transfer has to take place across liquid-liquid boundary. There are several types of contact-equipment in industrial use; basically there are two types of units. Those in which each individual stage is a separate unit and those in which several stages are integrated into one column. Multistage-columns can be simple spray or packed columns or can have stages equipped with various types of mixing devices separated by coalescence sections. The stage efficiency and the

throughput of such devices are a strong function of the mass-transfer and the coalescence rate.

Another important point worth mentioning is the fact that high intensity mixing is required in order to form small drops and good contact between the phases in slow mass-transfer systems. However, the shear stress induced by such a mixing can, in many cases, damage high molecular weight molecules. In addition, the intense mixing forms fine dispersions which reduces the coalescence rate, or in the presence of surface active impurities, may even cause a "stable emulsion", one of the operating hazards of solvent extraction equipment. In the presence of surface-active impurities, this intense mixing may even cause emulsion formation, which is a common problem in the pharmaceutical industry, where the desired products are frequently extracted from fermentation broths containing surface-active impurities. Furthermore, the active compounds to be extracted from the fermentation broths are often "imprisoned" in cell debris, which makes the penetration of solvents even more difficult to achieve.

It would be a novel approach with significant advantages to have contacting equipment and solvent systems that will operate with minimal or without any mechanical agitation and in which there will be no stable boundaries to slow down the mass-transfer and the coalescence rates.

Properties of solvent system with critical point of miscibility

As our whole approach, the present work is based on using partially miscible liquid solvents. A short review of their properties is as follows:

Two-component liquid system may be classified according to whether the components are completely or only partially miscible.

Consider two liquids A and B, exhibiting only partial miscibility. While complete miscibility is obtained whenever a small amount of A is added to B, as more A is added to the solution, eventually the limit of solubility of A in B at the current temperature is reached. Then, further addition of A will result in the appearance of two liquid phases that are saturated solutions of A in B and of B in A. Finally, sufficient addition of A will again bring the system to a condition of one liquid phase. Thus, for a substantial range of the system composition at a given temperature, two liquid phases of constant composition, the saturated solutions, will coexist. The variation in the composition of these saturated solutions with temperature is conveniently shown graphically in the so-called miscibility curves (sometimes also called solubility or coexistence curves).

In the case described in Figure 1 (Ullmann et al., 1995) which is typified by the system butanol-water, the

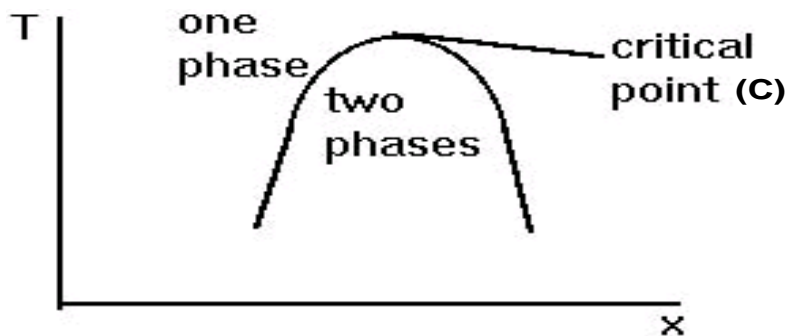


Figure 1. Upper critical solution temperature (UCST) (Ullmann et al., 1995).

solubilities of component A in component B and B in A increase with increase in temperature; so at some elevated temperature, at point C, the two conjugate solutions become identical and the interface between them consequently disappears. This point is termed the critical solution temperature (CST), or consolute temperature, and in the case described in Figure 1, point C is in fact an upper critical solution temperature (UCST). The physical explanation of the critical miscibility phenomena is based upon the interplay of intermolecular forces (Rowlinson, 1969; Domb and Green, 1972).

For example, the existence of UCST can be explained assuming that the A-B molecular bond is weaker than the individual interaction A-A and B-B; then at high temperatures (above UCST) the entropy effects are favored and complete miscibility results. At low temperatures the free energy of interactions is favored and phase separation occurs.

Explanations of the LCST (Domb and Green, 1972) revolve around the highly directional short-range interaction of the entities A and B as in the hydrogen bonding case. At low temperatures the decrease in free energy of solution due to specific interaction of A with B gives rise to miscibility. However, as temperature rises above the LCST, the entropy effects take over favoring a more random orientation of the entities.

The addition of even a small amount of a third component to a two-component liquid system may alter the CST considerably. Typically, when the third component is much more soluble in one of the binary mixture components, its addition raises the UCST (Hales and Green, 1966). When the third component distributes in roughly equal proportions between the two components, its addition tends to lower the UCST (Snyder and Eckert, 1973). Therefore water, for example, raises the UCST of methanol/n-hexane mixture (Rogers, 1969), whereas acetone, as a third component, lowers the UCST of methanol/cyclohexane by 3.5°C% of acetone dissolved (Cohen and Jacobs, 1984). In a similar way, the addition of a third component that is soluble in both liquids raises the LCST, and addition of a third component that is mainly soluble in one of the binary solution mixture components

lowers the LCST. Due to the addition of a third component to a two-liquid system and its distribution between the equilibrium phases, the critical composition will be altered as well. However, for a small amount of third component, the solvents mixture can be regarded as a pseudo two-component system, and the changes in the critical temperature and critical composition can be considered linear (Gunton et al., 1983; Cohn and Jacobs, 1984).

Solvent and solute distribution following phase transition

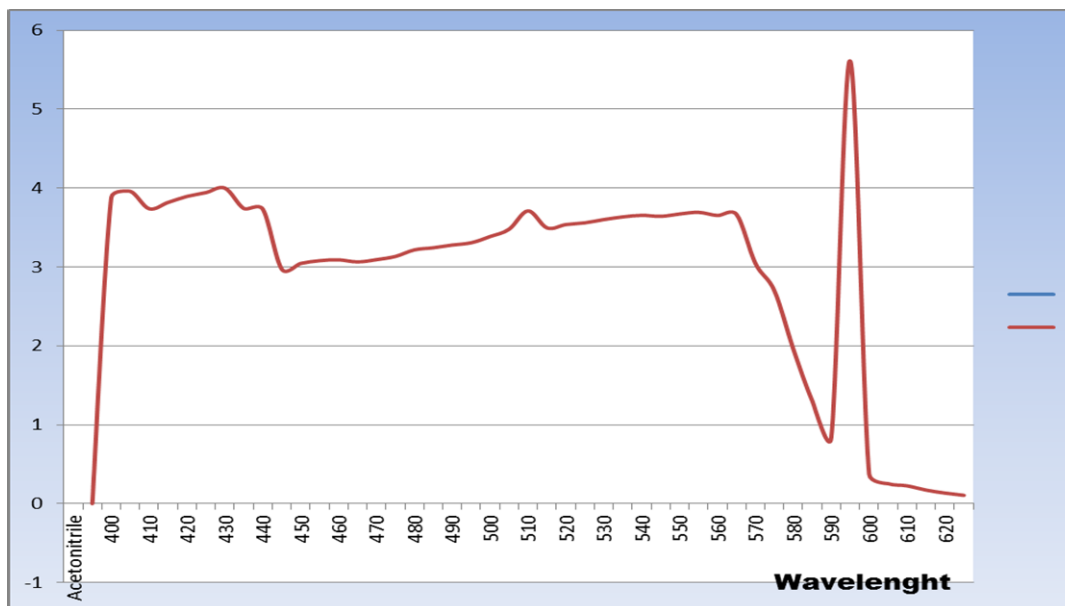
Selection of solvents and solute systems

Generally, the selection of solvent for liquid-extraction processes involves criteria such as capacity, selectivity, availability, physical properties, safety, and cost. When choosing a solvent for the PTE process two additional features are important. First, the deviation of the critical temperature of the mixtures from the ambient temperature should be small, since a large deviation would make the PTE process energy intensive. Secondly, it is advantageous to have as low a solvent concentration in the feed-rich phase as possible; this will minimize the need for solvent separation by distillation, and will also increase the distribution coefficient (Table 1).

In our experiments, the selection of a solvent system for the experiments is mainly affected by our need for easy and accurate experimental operation. Most experiments were conducted with a water-acetonitrile-toluene system. Water was selected as one of the components of our experimental system since it is frequently used as a feed solvent in many commercial extraction processes. Acetonitrile, which is commonly used as a solvent for HPLC analysis and to extract fatty acids from animal and vegetable oils, was selected as the second component. The acetonitrile-water system has an UCST at -0.5°C with 0.36 acetonitrile molar fraction (Figure 2 and Table 2). Toluene has been used as a third component to increase the CST to the desired operational level. Oil O Red was chosen as a model solute.

Table 1. Wavelengths, Transmittances and Absorbances.

Wavelength (nm)	100ppm of dye in acetonitrile		100ppm of dye in methanol	
	%T	A	%T	A
400				
405				

**Figure 2.** Absorbance vs Wavelength for Acetonitrile.

The use of a dye as a solute allows as easy, accurate and fast measurement of even very low dye concentration by means of light absorption spectrophotometry. A low solute concentration was preferred because it has a negligible effect on the solvents mutual miscibility and thus simplifies the performance computation of multi-stage extraction processes.

EXPERIMENTS

Measurement of solute concentration

The light absorption spectroscopy method is used to measure the dye concentration in the solvents. A Perkin Elmer UV/Vis spectrophotometer needs to be utilized for this purpose. Absorption spectra of the dye dissolved in methanol showed a maximum at a wavelength (Figure 3 and Table 3). This wavelength is unchanged whether the dye is dissolved in the acetonitrile-rich phase or water-rich phase of the acetonitrile-water-toluene system. Thus, the dye concentration, in each of the phase, can be obtained by diluting the sample with methanol as a reference solvent.

We will use the Beer-Lambert law to have absorbance data for our solutions. Beer-Lambert law states that the absorbance values for a particular solution are directly proportional to the concentration values of this solution and the path length of the light beam over

which the absorbance takes place.

Mathematically, this relationship can be written as:

$$A = \epsilon bc$$

Where A is the absorbance value for a solution at a particular wavelength, ϵ is the molar absorptivity of the solute at this wavelength in $\text{L mol}^{-1}\text{cm}^{-1}$, b is the length of the path of light through the solution in cm, and c is the concentration of the solution being analyzed in mol L^{-1} . Beer's law has many useful applications in analytical chemistry and related disciplines. It can be used in calculating concentrations of unknown solutions when molar absorptivity values are provided.

Experiment 1

- 1) The spectrophotometer should be turned on at least 20 min before any measurements are made.
- 2) Construct graphical plots of absorbance vs. wavelength (absorption spectra) for two different solutions.
- 3) Determine the wavelength at which maximum absorbance occurs for each solution.

Procedure

- 1) Dissolve 1 mg of Oil 0 Red in 10 mL of acetonitrile,

Table 2. Wavelengths and Absorbances for Acetonitrile.

Wavelength	Absorbance (A)
400	3.88
405	3.96
410	3.738
415	3.819
420	3.895
425	3.943
430	4
435	3.741
440	3.732
445	2.972
450	3.045
455	3.08
460	3.091
465	3.065
470	3.093
475	3.134
480	3.217
485	3.244
490	3.278
495	3.307
500	3.386
505	3.479
510	3.711
515	3.495
520	3.538
525	3.56
530	3.601
535	3.635
540	3.655
545	3.642
550	3.672
555	3.693
560	3.653
565	3.666
570	3.044
575	2.699
580	1.959
585	1.301
590	0.839
595	5.61
600	0.372
605	0.253
610	0.226
615	0.172
620	0.134
625	0.105

and 1 mg of Oil O Red in 10 mL of methanol. Now, you have two solutions with 100 ppm concentration of dye. Mix well by inverting the flask about 15 times.

2) Set the wavelength dial of the Spec 20 at 375 nm; perform 0%T adjustment with no test tube and 100% adjustment with distilled water in the test tube.

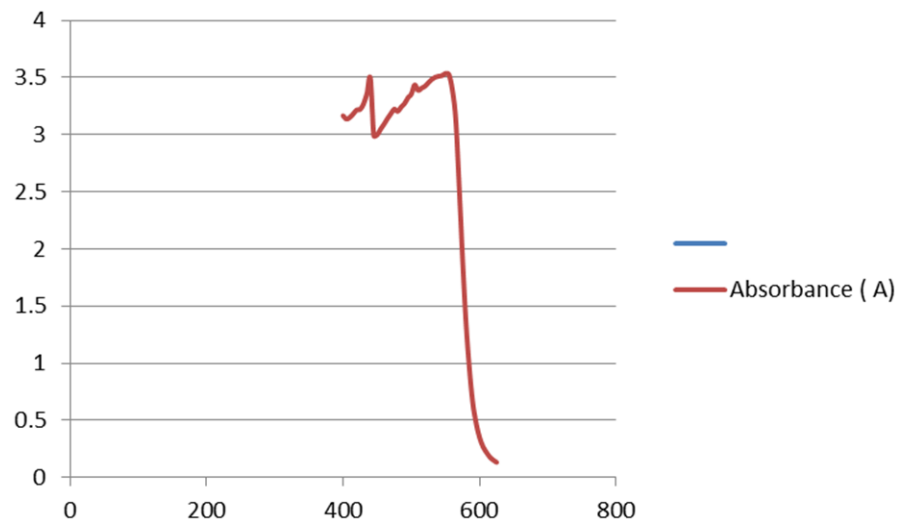


Figure 3. Absorbance vs Wavelength for Methanol.

Table 3. Wavelengths and absorbances for methanol.

Wavelength	Absorbance (A)
400	3.166
405	3.137
410	3.152
415	3.183
420	3.217
425	3.222
430	3.271
435	3.362
440	3.493
445	2.991
450	3
455	3.049
460	3.092
465	3.141
470	3.184
475	3.224
480	3.205
485	3.241
490	3.272
495	3.323
500	3.356
505	3.436
510	3.388
515	3.408
520	3.424
525	3.455
530	3.484
535	3.503
540	3.512
545	3.517
550	3.536

Table 3. Contd.

555	3.528
560	3.397
565	3.142
570	2.568
575	1.921
580	1.367
585	0.963
590	0.658
595	0.475
600	0.351
605	0.272
610	0.222
615	0.180
620	0.154
625	0.134

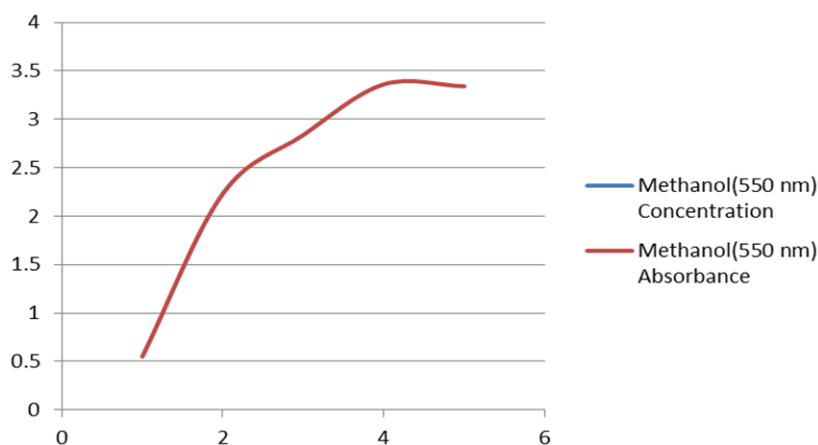


Figure 4. Absorbances vs Concentrations of methanol.

- 3) Obtain %T readings for each solution and record them in your notebook.
- 4) Turn the wavelength dial to 400 nm.
- 5) Repeat the adjustments and the procedure to obtain %T reading for each solution at 5 nm increments from 400 to 625 nm.

Treatment of data

1) You have to make a table in which you record %Transmittance (%T) and Absorbance values (A) for both solutions, using the formula

$$A = 2 - \log\%T.$$

2) Then, you have to plot the absorbance values versus the wavelength values for both solutions. Through this plot, you can determine the values of maximum

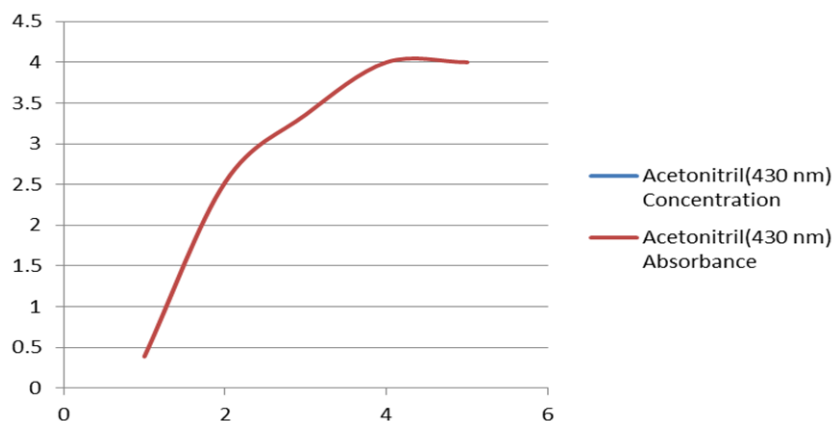
absorbance for both solutions. You have to record these values of maximum absorbance, since you have to use them in future experiments. Since Beer's law is more accurate, when absorbance for each concentration is measured around the wavelength of maximum absorbance, we have to include these values in future studies. We also need to include the values of wavelengths at the intersection points of the two curves. In addition, we include the minimum value of the wavelength for both solutions.

Results of Experiment 1

Values of absorbances were collected for acetonitrile and methanol using different wavelengths with increments of 5 nm (Figure 4 and Table 4). The wavelength at which

Table 4. Concentrations vs Absorbances for Methanol and Acetonitrile.

Concentration (ppm)	Absorbance
Methanol (550 nm)	
50	0.552
100	2.233
150	2.839
200	3.362
250	3.342
Acetonitrile (595 nm)	
50	0.389
100	2.528
150	2.017
200	4
250	4

**Figure 5.** Absorbances vs Concentrations of acetonitrile.

the absorbance has the maximum value was picked for the next experiment.

Experiment 2

- 1) Construct Beer's Law plots (absorbance vs. concentration) for different concentrations of Oil 0 Red in acetonitrile and methanol at different wavelength (Figure 5).
- 2) Determine whether linear relationship between absorbance and concentration is true for these solutions of different concentrations.

Procedure

- 1) Prepare samples of 50, 100, 150, 200 and 250 ppm solutions.
- 2) Use the HP diode array spectrophotometer to obtain absorbance values for the five solutions mentioned above

- at the wavelength at which the absorbance is maximum.
- 3) Record the absorbance values for each concentration and construct Beer's law plots (absorbance versus concentration).

Treatment of data

You have to make two tables in which you record absorbance values for different concentrations for both solutions at the wavelength maximum. Then, you can plot absorbance values versus concentration values.

Results of Experiment 2: Phase transition extraction (PTE)

Representation of concept: Based on the properties of mixtures with critical point of miscibility, a new separation

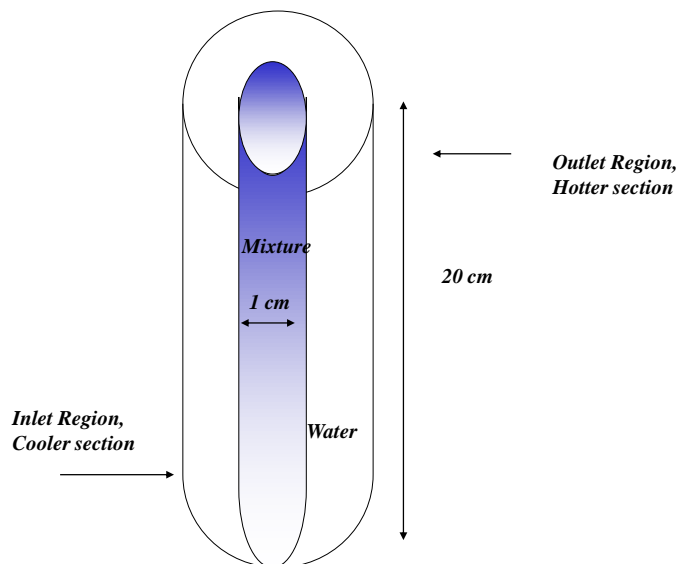


Figure 6. Condenser tube.

process (PTE) is used to separate our mixtures. The novel process capitalizes on the phase transition of such mixtures, especially on the fact that with a relatively small change in temperature one can go from one completely mixed phase to two phases with differing compositions (Figure 1). Our liquid systems form a homogeneous solution above the critical point and two separate phases below the critical point.

Phase separation rate during phase transition: We can test the phase separation rate by performing a series of batch experiments. In these experiments we measure the time needed to complete a full phase separation of a mixture of solvents following a phase transition, and we compare this time with the separation time of the isothermally-mixed mixture.

For all the solvent systems, when the homogenous solvent mixtures are separated by temperature quench, the phase separation is very fast and is complete in one minute.

An experimental setup was designed and built to allow the observation of the phase separation process consisting in a condenser tube (Figure 6) which is 20 cm long and 1 cm in diameter. This experimental setup allows the observation of the motion of individual droplets in a size range of 0.5 mm of diameter and up. The condenser tube is closed on both ends; the temperature is controlled by currently heat transfer liquid trough the cooling system of the condenser, using two constant temperature reservoirs- one hot and one cold, keeping the temperature of each reservoir constant at the desired value and allowing a fast switch between the hot and the cold loops.

In our experiments we use a liquid mixture composed

of water, acetonitrile and toluene; it has a critical volumetric composition of 38% water, 58% acetonitrile, 4% toluene and it undergoes phase transition at critical temperature of 35°C. At ambient temperature, this mixture separates into two phases with a density difference $\Delta\rho_l = 7 \times 10^2 \text{ g/cm}^3$ and surface tension $\sigma_l = 1.3 \text{ dyne/cm}$, so that its capillary length is $Rc_l = 1.3 \text{ mm}$. Here, water is the continuous phase. In addition, 50 ppm of Oil 0 Red is added to the mixture to enhance the visualization of the two phases as they separate. When dissolved in such small percents, this dye does not change the phase diagrams of the mixture, or the characteristic of the phase separation process. All the solvents must be HPLC grade, while water is double distilled.

Procedure

- 1) We start with the mixture in its phase-separated state at a constant temperature of 20°C. Then, the solution is first heated to 38°C (that is, well above its critical temperature), mixed thoroughly and finally quenched back to 7°C, with a quench rate of about 3°C/s. This quenching is achieved by circulating cooling water at 7°C through the outer chamber of the condenser.
- 2) The mixture reaches complete separation before it becomes completely cooled. The time reported in all experiments is measured from the moment the temperature crosses the miscibility curve.
- 3) Prepare the same mixture, and heat it up to 38°C; then let it cool down at room temperature. Compare the times of complete separation with the PTE times of separation (Figure 7).

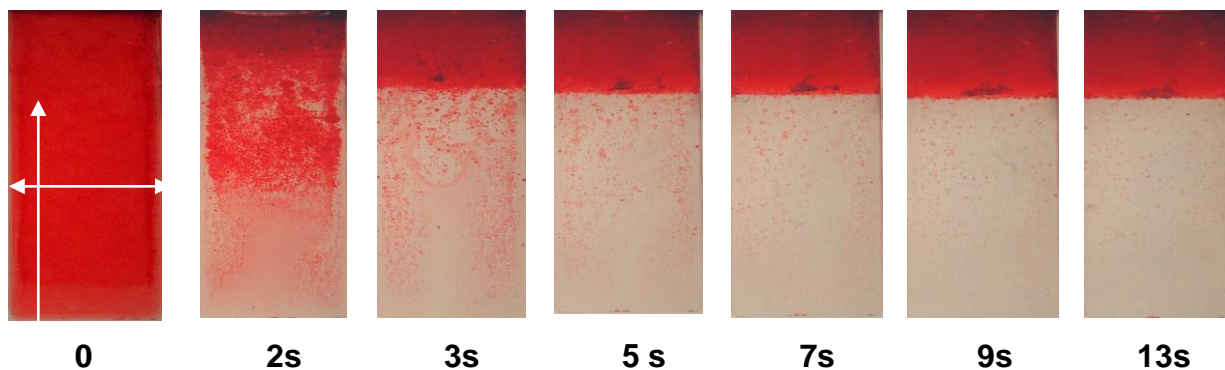


Figure 7. Phase transition extraction process (PTE).

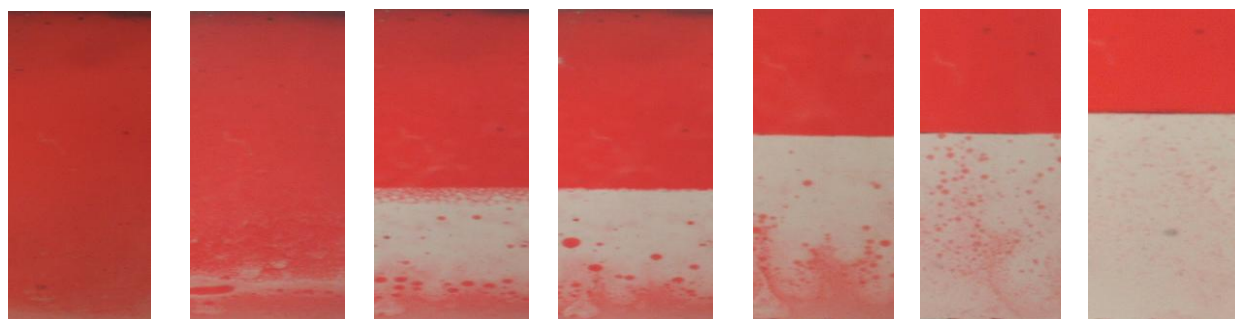


Figure 8. Liquid liquid extraction process (LLE).

Results of Experiment 2

In this study we compared two different processes involving mixtures of two partially miscible liquids, initially in their two-phase state: in the former, the mixture is agitated isothermally (LLE) (Figure 8), while in the latter, it is heated and cooled across its miscibility curve, inducing phase transition (PTE). The most important result of that study is that, while, as expected, the coalescence rate and settling time in the first case are strongly influenced by the presence of emulsifiers, this is not so when the mixture undergoes phase transition. In fact, in this case we found that phase separation is rapid, irrespective of whether or not surface-active compounds are added.

Conflict of Interest

The authors have not declared any conflict of interest.

REFERENCES

Alegert S (1988). Developments in solvent extractions. *J. membrane sci.* P. 35.

- Cohen P, Jacobs C (1984). The clinician's illusion. *Arch. Gen. Psychiatry* 41(12):1178-1182. <http://dx.doi.org/10.1001/archpsyc.1984.01790230064010>
- Domb C, Green MS (Eds.) (1972). *Phase transitions and critical phenomena*. Academic Press, London and N.Y. 2:18.
- Gunton J, SanMiguel M, Sahni P (1983). *Phase transition and critical phenomena*, Domb and Lebowitz Eds, Academic press, P. 8.
- Hales AL, Green RWE (1966). Seismic refraction measurements in the southwestern Indian Ocean. *J. Geophys. Res.* 71:1637-1647. <http://dx.doi.org/10.1029/JZ071i006p01637>
- Hanson C (1971), *Handbook of solvent extraction*, Wiley-Interscience, New York, ISBN 0471041645.
- Lo T, Baird I, Hanson C (1983). *Handbook of solvent extraction*, Wiley-Interscience, New York.
- Rogers CR (1969). *Freedom to Learn*. Columbus, OH: Merrill.
- Rowlinson JS (1969). *Liquids and liquid mixtures*. 2d ed. Plenum Press in New York . P. 371.
- Snyder RB, Eckert CA (1973). Chemical kinetics at a critical point. *AIChE J.* 19:1126-1133. <http://dx.doi.org/10.1002/aic.690190608>
- Treybal RE (1963). *Liquid extraction*, McGraw Hill, New York, NY. P. 666.
- Ullmann A, Ludmer Z, Shinnar R (1995). Phase transition extraction using solvents mixtures with a critical point of miscibility. *AIChE J.* 41:489. <http://dx.doi.org/10.1002/aic.690410307>

Full Length Research Paper

Electrical properties and crystal structure of Y123, Y358 and Y257/Y211 composite bulk superconductors

Kruaehong T.

Department of Physics, Faculty of Science and Technology, Suratthani Rajabhat University, Surat Thani province, 84100, Thailand.

Received 18 July, 2014; Accepted 25 August, 2014

The Y123, Y358 and Y257 bulk superconductors mixed with various ratio of non-superconducting Y211 (Y_2BaCuO_5) were synthesized by solid state reaction. The physical properties of pellets were investigated by d.c. four-probes measurement. The crystal structure was determined using powder X-ray diffraction and the characteristic peaks were determined using the Rietveld full-profile analysis method. Results showed that the $T_{c,onset}$ and $T_{c,offset}$ decreased with the increasing of Y211 doping. The samples consist of both superconducting phase and the non-superconducting phase. The lattice parameter of Y211 doped samples showed lower c direction than pure samples. The superconducting phase decreased with increasing Y211 content. The non-superconducting phases consists of Pccm ($Ba_2Cu_3O_6$) and Im-3m ($BaCuO_2$) respectively. According to the percentage of superconducting phase, the anisotropy increased with Y211 contents.

Key words: Y-based superconductors, Y211, Rietveld method.

INTRODUCTION

Since $YBa_2Cu_3O_7$ (Y123) superconductor which has highest critical temperature at 93K was found in 1987 (Wu et al., 1987), many researchers have performed vigorously to improve its superconducting properties and the results have been applied to the fabrication of various film or bulk type superconductors. In 2009, the $Y_3Ba_5Cu_8O_{18}$ (Y358) was found (Alibadi et al., 2009). This is the highest critical temperature of Y-based superconductor that has highest critical temperature at 102K. In 2013, Kruaehong (2013) could synthesize the new superconductors, $Y_2Ba_5Cu_7O_{15}$ (Y257) by solid state reaction. This superconductor has highest critical temperature about 94K. Because superconducting

properties of the Y123, Y358, and Y257 can be performed in liquid nitrogen, this cheap cryogenic medium makes the materials promising in many fields such as superconducting magnetic bearings (Jiqiang et al., 2012), superconducting electric motors (Hiroyuki and Yuichi, 2001), magnetic separation devices (Oka et al., 2013), non-contact transport systems (Smith and Jr. Dolan, 2013), flywheel energy storage systems (Arai et al., 2013) and permanent magnets with high trapped field (Liu et al., 2011) operating above 77K (Moon and Chang, 1990; Hull, 2001).

It is well known that Y211 (Sandiumeng et al., 1997) which is the second phase of the Y123, Y211 doping,

E-mail: kruaehong@hotmail.com

Author(s) agree that this article remain permanently open access under the terms of the [Creative Commons Attribution License 4.0 International License](https://creativecommons.org/licenses/by/4.0/)

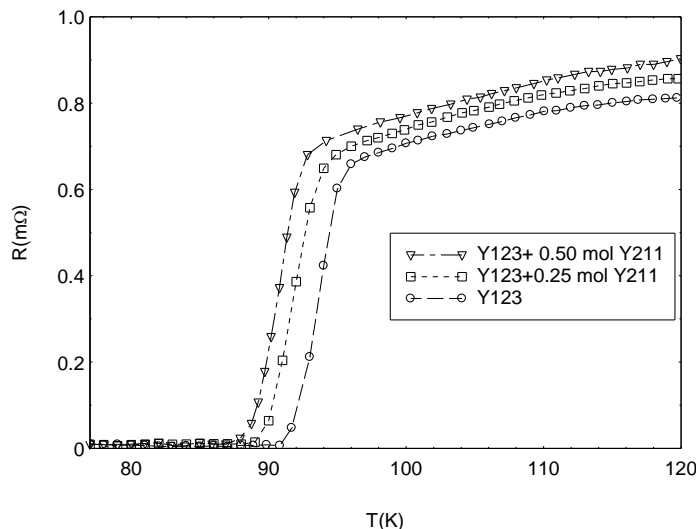


Figure 1. Graph plot between resistance and temperature of Y123 and Y211 doped.

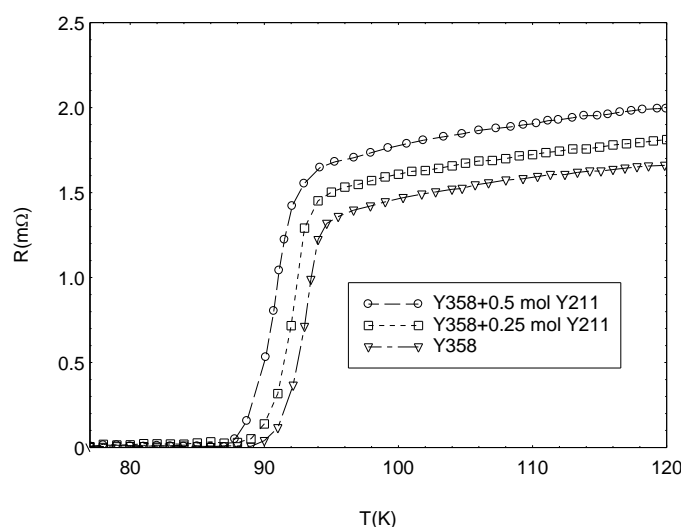


Figure 2. Graph plot between resistance and temperature of Y358 and Y211 doped.

plays an important role in enhancing the superconducting properties of Y123 superconductors due to the increasing of high critical current density (J_c) (Fujishiro et al., 2003). Therefore, The crystal structure of Y123/Y211 composites have been attentively investigated by many research groups (Mucha et al., 2010; Endo et al., 1996; Dias et al., 2009; Yu et al., 1997; Kim and Kim, 2000).

In this present work, the influence of Y_2BaCuO_5 (Y211) doping in the Y123, Y358 and Y257 superconductors were reported. Y123, Y358 and Y257 superconductors were doped with 0, 0.25 and 0.50 mol of Y_2BaCuO_5 (Y211), critical temperature, phase composition and lattice parameter of the samples were compared.

Electrical measurements were carried out using d.c. four-probes technique. Structural analysis was analyzed by D8 Advance Discovery with $CuK\alpha$ radiation.

MATERIALS AND METHODS

The Y123, Y358 and Y257 polycrystalline superconductors and non-superconducting (Y211) were calcined and sintered in a square furnace under air system by solid state reaction. The high-purity (99.99%) raw materials of Y_2O_3 (99.99%), $BaCO_3$ (99.99%), and CuO (99.99%) powders were used as start materials. Raw materials of Y123, Y358, Y257 and Y211 were mixed with different atomic ratio ranging from 1:2:3, 3:5:8, 2:5:7 and 2:1:1, respectively. Firstly, the Y123, Y358, Y257 and Y211 powders were calcined at $950^\circ C$ and keep at that temperature for 24 h, then reduced to $100^\circ C$. Calcinations were repeated twice with intermediate grinding to obtained the black powder of Y123, Y358, Y257 powder and the green powder of Y211 powder. The Y211 of 0 mol, 0.25 mol, 0.50 mol were mixed to Y123, Y358 and Y257. The mixed powders were calcined at $950^\circ C$ and kept at that temperature for 24 h, then reground and pressed in to pellet of 30 mm in diameter and about 3 mm thickness under 2,000 psi pressure. Finally, the obtained specimens were sequentially sintered at $950^\circ C$ and kept at that temperature for 24 h and annealed at $500^\circ C$ for 24 h in the air.

The physical properties were analyzed by the electrical resistance and XRD diffractometer. The resistance as a function of temperature was set in a range of 77 to 120 K by using liquid nitrogen and measured by a standard d.c. four-probes method by means of a closed-cycle cryostat at low temperature down to 77K. Both voltage and current contacts were made with silver paint to minimize the contact resistance. A temperature value, where the resistance starts to increase significantly, was determined to be the onset critical temperature (T_c onset) of the sample whereas the offset transition temperature (T_c offset) was defined as the temperature at which $R=0 \Omega$.

The crystal structure was investigated by X-ray diffraction (XRD). Data were collected using a D8 Advance Discovery diffractometer with $CuK\alpha$ target giving a monochromatic beam with wavelength 1.5416 \AA in the range of $2\theta = 10-90^\circ$ at a scan speed of 3.4/min and step increment of 0.019° at room temperature. The lattice parameter (a , b and c) phase compositions, and space group were computed from the Rietveld full-profile analysis method (Rodriguez-Carvajai, 2001).

RESULTS AND DISCUSSION

Electrical resistance measurements

The critical temperature of the bulk samples of Y123, Y358 and Y257 and Y211 composite were investigated by aid of the dc electrical resistivity measurements using a current density of $3.82 \times 10^{-3} A/m^2$ and the temperature measured by thermocouple type K. The results are illustrated in Figures 1 to 3. The transition curves of the samples from the superconducting state to normal state exhibit the double-step behavior in all samples. Table 1 shows the onset critical temperature (T_c onset) and offset critical temperature (T_c offset). The samples exhibit metallic behavior above the zero resistivity transition temperature value. Moreover, it is obvious from the table that both T_c offset and T_c onset value of the Y123, Y358

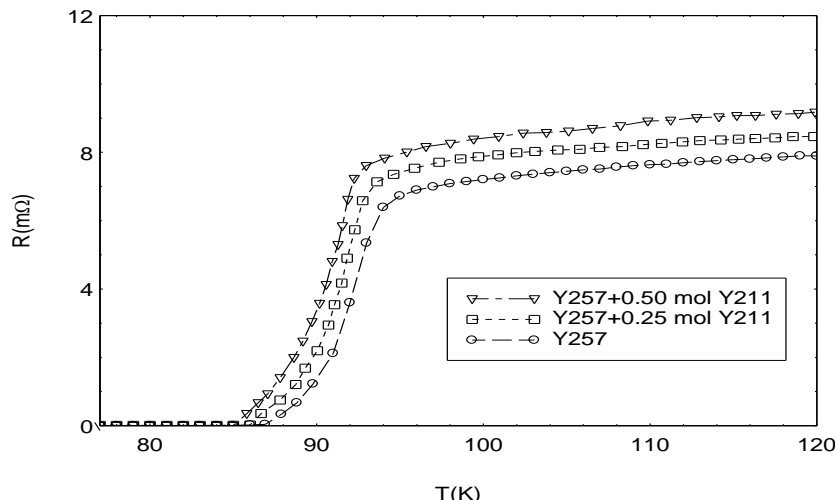


Figure 3. Graph plot between resistance and temperature of Y257 and Y211 doped.

Table 1. The T_c summation of the samples.

Samples	T_c offset (K)	T_c onset (K)
Y123	90.82	95.97
Y123+0.25molY211	89.99	94.90
Y123+0.50molY211	86.84	92.80
Y358	87.92	94.65
Y358+0.25molY211	86.98	93.00
Y358+0.50molY211	85.95	92.07
Y257	86.88	93.97
Y257+0.25molY211	85.95	93.61
Y257+0.50molY211	84.98	92.21

and Y257 doped with Y211 have lower value than the pure ones. The result is consistent with Kruaehong et al. (2013a, b). They mixed Y3-8-11 and Y7-11-18 superconductors with Y211 powder and his result showed that the critical temperature of Y3-8-11 and Y7-11-18 decreased with increasing Y211 content. This is because of poor thermal conductivity of Y211. In addition, Y211 also causes more scattering of phonon and quasi particle on the number of scattering centers (Jezowski et al., 2000).

The result of this work emphasis only on critical temperature of the sample, however, since high critical current density is considered to be one of the most important property of superconductor, thus the study on critical current density and critical magnetic field should be investigated in further study.

XRD measurement

The XRD spectra of the Y123, Y358, Y257 and Y211

composite samples are shown in Figures 4 to 12 respectively. The Rietveld full-profile analysis method was used to determine the orthorhombicity structure, phase compositions, and space groups. The difference between the experimental and calculated pattern is shown in the blue lines of the figures. Our samples exhibited the polycrystalline with the changing intensity of diffraction lines. The samples are composed of both superconducting phase and non-superconducting phases. The superconducting phase corresponds with orthorhombic structure and the non-superconducting phase shows various crystal structures. Table 2 shows percentage of the superconducting phase and non-superconducting phase in the samples. The Pmmm space group corresponds with the superconducting phase while the other space groups of the non-superconducting phase are composed of Pccm ($\text{Ba}_2\text{Cu}_3\text{O}_6$) and Im-3m (BaCuO_2) respectively. Additionally, Tables 3 and 4 show the lattice parameter of the superconducting phase and non-superconducting phases, respectively. The XRD pattern of the pure Y123

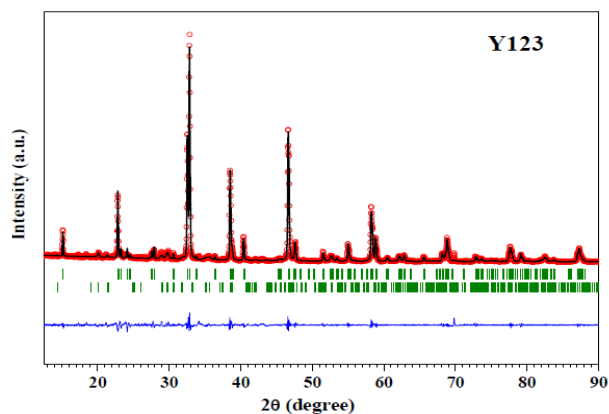


Figure 4. The XRD spectra of the pure Y123 superconductor. Experimental (o) are point on solid line, calculated (solid line) and the vertical ticks below the curve indicate the Bragg positions.

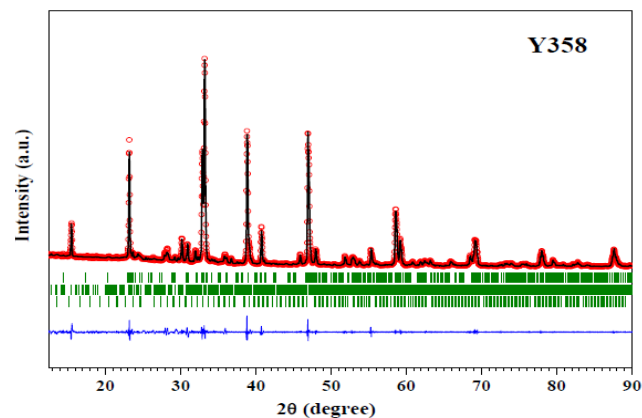


Figure 7. The XRD spectra of the pure Y358 superconductor. Experimental (o) are point on solid line, calculated (solid line) and the vertical ticks below the curve indicate the Bragg positions.

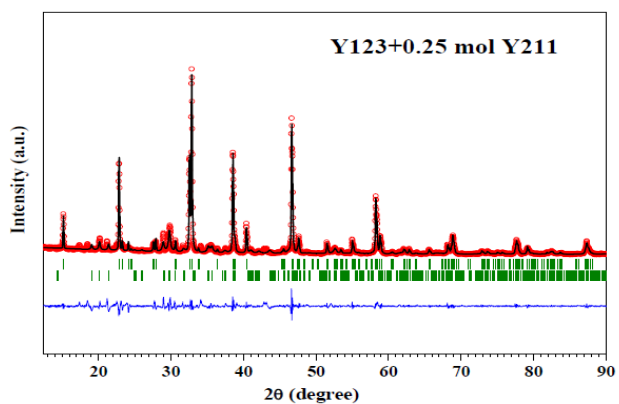


Figure 5. The XRD spectra of Y123+0.25 mol Y211 composite superconductor. Experimental (o) are point on solid line, calculated (solid line) and the vertical ticks below the curve indicate the Bragg positions.

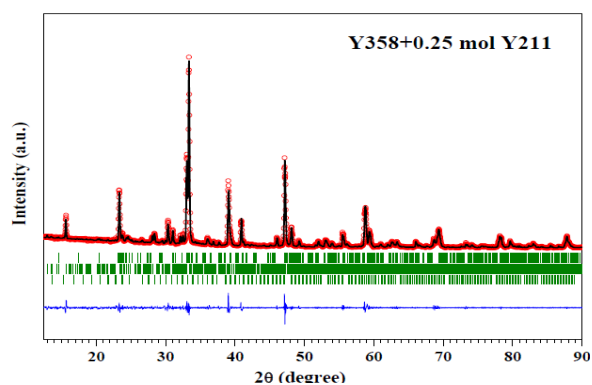


Figure 8. The XRD spectra of Y358+0.25 mol Y211 composite superconductor. Experimental (o) are point on solid line, calculated (solid line) and the vertical ticks below the curve indicate the Bragg positions.

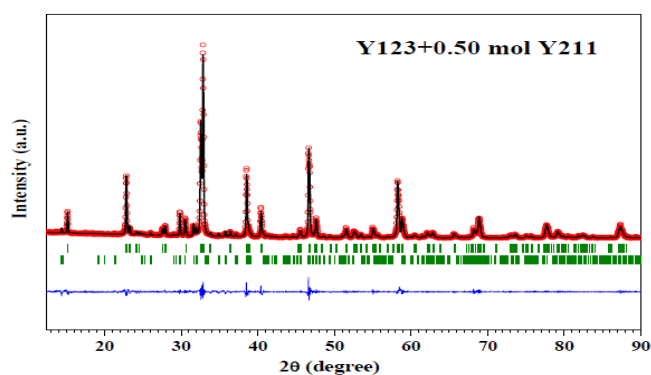


Figure 6. The XRD spectra of Y123+0.50 mol Y211 composite superconductor. Experimental (o) are point on solid line, calculated (solid line) and the vertical ticks below the curve indicate the Bragg positions.

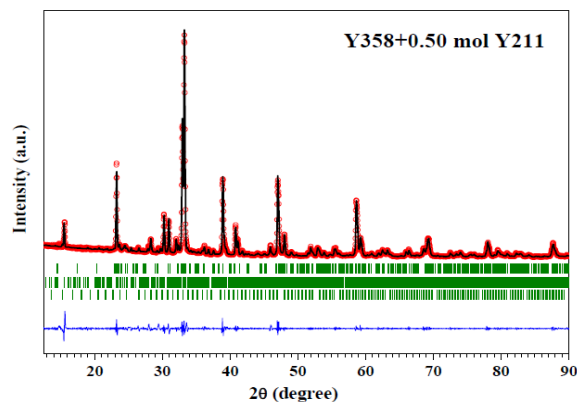


Figure 9. The XRD spectra of Y358+0.50 mol Y211 composite superconductor. Experimental (o) are point on solid line, calculated (solid line) and the vertical ticks below the curve indicate the Bragg positions.

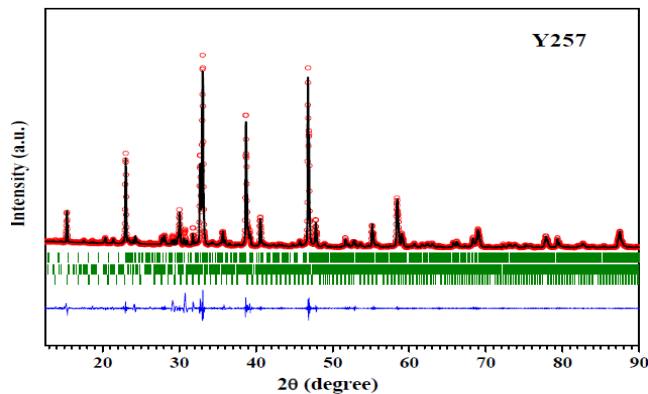


Figure 10. The XRD spectra of pure Y257 superconductor. Experimental (o) are point on solid line, calculated (solid line) and the vertical ticks below the curve indicate the Bragg positions.

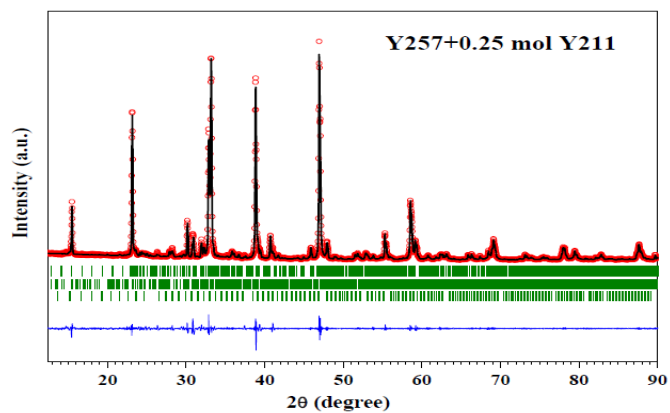


Figure 11. The XRD spectra of pure Y257+0.25 mol Y211 superconductor. Experimental (o) are point on solid line, calculated (solid line) and the vertical ticks below the curve indicate the Bragg positions.

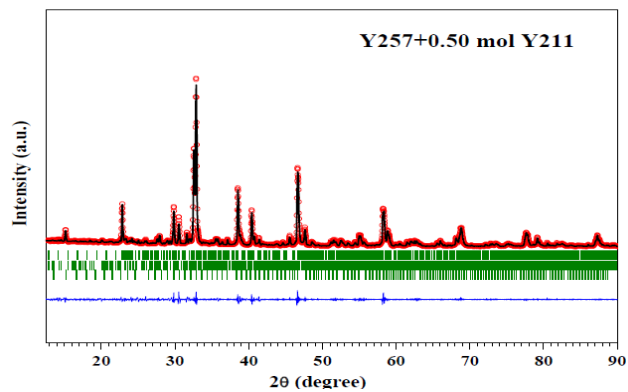


Figure 12. The XRD spectra of pure Y257+0.50 mol Y211 superconductor. Experimental (o) are point on solid line, calculated (solid line) and the vertical ticks below the curve indicate the Bragg positions.

Table 2. The percentage phase composition.

Samples	Percentage phase composition (%)		
	Superconducting phase, Pmmm	Non-superconducting phase	
		Ba ₂ Cu ₃ O ₆ , Pccm	BaCuO ₂ , Im-3m
Y123	90	6	4
Y123+0.25molY211	82	7	11
Y123+0.50molY211	80	12	8
Y358	25	55	20
Y358+0.25molY211	20	40	40
Y358+0.50molY211	15	35	50
Y257	14	36	50
Y257+0.25molY211	12	40	48
Y257+0.50molY211	10	45	45

Table 3. The lattice parameters of the superconducting phase.

Samples	Lattice parameters			Anis=200 [(b-a)/(b+a)]
	a(Å)	b(Å)	c(Å)	
Y123	3.81710 0.00008	3.88430 0.00009	11.68000 0.00021	1.73
Y123+0.25molY211	3.81590 0.00017	3.88540 0.00090	11.67590 0.00023	1.78
Y123+0.50molY211	3.81660 0.00015	3.88670 0.00038	11.67390 0.00029	1.80
Y358	3.82257 0.00009	3.87603 0.00004	30.66149 0.00044	1.38
Y358+0.25molY211	3.82884 0.00027	3.88363 0.00026	30.52480 0.00176	1.42
Y358+0.50molY211	3.77715 0.00009	3.84602 0.00012	30.39207 0.00070	1.80
Y257	3.80225 0.00008	3.86696 0.00009	26.38292 0.00129	1.68
Y257+0.25molY211	3.81932 0.00006	3.89151 0.00004	25.86840 0.00095	1.87
Y257+0.50molY211	3.81011 0.00009	3.88957 0.00009	25.70966 0.00133	2.06

revealed that it is composed highest content of superconducting phase comparing to the doped samples. Besides, in case of increasing non-conducting phase the lower *c* direction was occurred. The main peaks of Y358 and Y257 were similar with Y123 superconductor. The

anisotropic of the samples are equal to $200(b-a)/0.5(b-a)$. Moreover, the more content of Y211 doping causes more anisotropic of the samples (Table 3).

It is important to note that the XRD could not detect Y211 in the final samples. This may be due to the

Table 4. The lattice parameter of the non-superconducting phase.

Samples	Non-superconducting phase								
	Y ₂ BaCuO ₅ ,Pbnm			BaCuO ₂ ,Im-3m			Ba ₂ Cu ₃ O ₆ ,Pccm		
	a(Å)	b(Å)	c(Å)	a(Å)	b(Å)	c(Å)	a(Å)	b(Å)	c(Å)
Y123	7.13074	12.27472	5.61281	-	-	-	-	-	-
	0.00157	0.00314	0.00101						
Y123+0.25molY211	7.13609	12.27148	5.60504	-	-	-	-	-	-
	0.00134	0.00186	0.00086						
Y123+0.50molY211	7.13139	12.17139	5.65701	-	-	-	-	-	-
	0.00018	0.00045	0.00017						
Y358	-	-	-	18.44041	18.44041	18.44041	13.07853	20.72125	11.44339
				0.00157	0.00157	0.00157	0.00019	0.00029	0.00019
Y358+0.25molY211	-	-	-	18.31984	18.31984	18.31984	12.94864	20.51307	11.33181
				0.00030	0.00030	0.00030	0.00023	0.00032	0.00015
Y358+0.50molY211	-	-	-	18.37572	18.37572	18.37572	13.05474	20.71643	11.42290
				0.00091	0.00091	0.00091	0.00021	0.00040	0.00018
Y257	-	-	-	18.23857	18.23857	18.23857	12.97630	20.56757	11.38094
				0.00047	0.00047	0.00047	0.00017	0.00026	0.00017
Y257+0.25molY211	-	-	-	18.41250	18.41250	18.41250	13.04191	20.71064	11.43900
				0.00169	0.00169	0.00169	0.00017	0.00032	0.00012
Y257+0.50molY211	-	-	-	18.47248	18.47248	18.47248	13.02902	20.63760	11.42583
				0.00086	0.00086	0.00086	0.00019	0.00027	0.00016

preparing process that the samples were calcined at 950°C. Such high temperature may transform the Y211 to be other substances such as BaCuO₂ and Ba₂Cu₃O₆.

Conclusion

The Y123, Y358 and Y257 superconductors and non-superconducting of Y211 were synthesized by solid state reaction. The black Y123, Y358 and Y257 and the green Y211 were obtained. The Y211 of 0, 0.25 and 0.50 mol were mixed with Y123, Y358 and Y257 to their superconductors. The mixed powders were calcined and sintered. The critical temperature of the T_c onset and T_c offset of samples were investigated by d.c. four-probes method and crystal structure were carried out by powder X-ray diffraction with Rietveld full-profile analysis method for determining the phase composition, lattice parameters of the superconducting phase, non-superconducting phase and space group. The results indicated that the T_conset and T_coffset of the samples lower with increasing Y211 doping. The samples consist of both superconducting and non-superconducting phase. The lattice parameter of pure samples has longer *c* direction than Y211 doped samples. The superconducting phase

decreased with increasing Y211 doping. There are three types of non-superconducting phases in the samples, Y211, BaCuO₂ and Ba₂Cu₃O₆ with Pbnm, Im-3m and Pccm, respectively. According to the percentage of superconducting phase, the anisotropy increased with more Y211 contents.

Conflict of Interest

The author has not declared any conflict of interest.

ACKNOWLEDGEMENTS

The author would like to thank Professor Dr. Suthat Yoksan for the useful discussions. Faculty of Science and Technology, Suratthani Rajabhat University and Faculty of Science, Srinakharinwirot University were also acknowledged.

REFERENCES

Alibadi A, Farschi YA, Akhavan MA (2009). New Y-based HTSC with T_c above 100 K. Physica C. 469:2012-2014.

- <http://dx.doi.org/10.1016/j.physc.2009.09.003>
- Arai Y, Seino H, Yoshizawa K, Nagashima K (2013). Development of Superconducting Magnetic Bearing with Superconducting Coil and Bulk Superconductor for Flywheel Energy Storage System. *Physica C*. 494:250-254.
<http://dx.doi.org/10.1016/j.physc.2013.04.039>
- Dias FT, Vieira VN, Pureur P, Rodrigues Jr P, Obradors X (2009). Fluctuation Conductivity along the c-axis and parallel to the ab-planes in melt-textured $\text{YBa}_2\text{Cu}_3\text{O}_{7-\delta}$ samples doped with Y211 phase. *Physica B*. 404:3106-3108.
<http://dx.doi.org/10.1016/j.physb.2009.07.058>
- Endo A, Chauhan HS, Shiohara Y (1996). Entrapment of YBa_2CuO_5 Particle in Melt-Textured $\text{YBa}_2\text{Cu}_3\text{O}_{7-\delta}$ Crystal and its Effect on J_c . *Physica C*. 273:107-119.
[http://dx.doi.org/10.1016/S0921-4534\(96\)00595-3](http://dx.doi.org/10.1016/S0921-4534(96)00595-3)
- Fujishiro H, Teshima H, Ikebe M, Noto K (2003). Thermal Conductivity of YBaCuO Bulk Superconductors Under Applied Field, Effect of Content and Size of Y211 Phase. *Physica C* 392-396:171-174.
[http://dx.doi.org/10.1016/S0921-4534\(03\)01104-3](http://dx.doi.org/10.1016/S0921-4534(03)01104-3)
- Hiroyuki O, Yuichi T (2001). Study and Electric Motor with Bulk Superconductors in the Rotor. *J. Mater. Proc. Technol.*108:148-151.
[http://dx.doi.org/10.1016/S0924-0136\(00\)00744-5](http://dx.doi.org/10.1016/S0924-0136(00)00744-5)
- Hull JR (2001). Superconducting Bearings, *Superconductor Sci. Technol.* 13:13R1.
- Jezowski A, Rogacki K, Puig T, Obradors X (2000). Anisotropy of the thermal conductivity of melt-textured Y123/Y211 composites. *Physica B*.284-288:1015-1016.
[http://dx.doi.org/10.1016/S0921-4526\(99\)02360-1](http://dx.doi.org/10.1016/S0921-4526(99)02360-1)
- Jiqiang T, Jiancheng F, Shuzhi SG (2012). Role of superconducting magnetic bearings and active magnetic bearing in attitude control and energy storage flywheel. *Physica C*.483:178-185.
<http://dx.doi.org/10.1016/j.physc.2012.07.007>
- Kim SJ, Kim HG (2000). Effect of 211 Inclusions on zone melt-textured (RE/Y)Ba-Cu-O Superconductors. *Physica C*. 338:110-114.
[http://dx.doi.org/10.1016/S0921-4534\(00\)00211-2](http://dx.doi.org/10.1016/S0921-4534(00)00211-2)
- Kruaehong T, Preparation and Characterization of the new Y257 Superconductors. *Advan. Mater. Res.* 770:22-25.
- Kruaehong T, Sujinnapram S, Nilkamjon T, Ratreng S, Udomsamuthirun P (2013a). Some properties of Y3-8-11/Y211 Composite Bulk Superconductors. *KMITL Sci. Technol. J.* 13:38-41.
- Kruaehong T, Sujinnapram S, Nilkamjon T, Ratreng S, Udomsamuthirun P (2013b). Investigate the properties of Y211 doping effect in the new superconducting $\text{Y}_7\text{Ba}_{11}\text{Cu}_{18}\text{O}_y$ Compound. *Advan. Mater. Res.* 770:26-29.
<http://dx.doi.org/10.4028/www.scientific.net/AMR.770.26>
- Liu W, Wang JS, Liao XL, Zheng SJ, Ma GT, Zheng J, Wang SY (2011). Levitation performance of the magnetized bulk high- T_c superconducting magnet with different trapped fields. *Physica C*. 471:156-162.
<http://dx.doi.org/10.1016/j.physc.2010.12.016>
- Moon FC, Chang PZ (1990). High-speed rotation of magnets on high- T_c superconducting bearings, *Appl. Phys. Lett.* 56:397-399.
<http://dx.doi.org/10.1063/1.102795>
- Mucha J, Rogacki K, Misiorek H, Jezowski A, Wisniewski A, Puzniak R (2010). Influence of the Y211 Phase on Anisotropic Transport Properties and Vortex Dynamics of Melt-Textured Y123/Y211 Composite. *Physica C*. 470:S1009-S1010.
<http://dx.doi.org/10.1016/j.physc.2010.01.063>
- Oka T, Kimura T, Mimura D, Fukazawa H, Fukui S, Ogawa J, Sato T, Ooizumi M, Yokoyama K, Tsujimura M, Terasawa T (2013). Magnetic precipitate separation for Ni Plating Waste Liquid Using HTS Bulk Magnet. *Physica C*. 484:325-328.
<http://dx.doi.org/10.1016/j.physc.2012.03.010>
- Rodriguez-Carvajai J (2001). An introduction to the program FULLPROF Laboratoire Leon Brillouin. P. 35.
- Sandiumeng F, Martinex B, Obradors X (1997). Tailoring of microstructure and critical current in directionally solidified $\text{YBa}_2\text{Cu}_3\text{O}_{7-\delta}$ Superconductor *Sci. Technol.* 10:A93-119.
<http://dx.doi.org/10.1088/0953-2048/10/7A/008>
- Smith CW, Jr. Dolan PJ (2013). Determining transport parameters for superconductor/normal metal point contact at fixed temperature from conductance versus magnetic field data. *Physica C*. 471:285-289.
<http://dx.doi.org/10.1016/j.physc.2011.02.007>
- Wu K, Ashburn JR, Torng CJ, Hor PH, Meng RL, Gao L, Huang ZJ, Wang YQ, Chu CW (1987). Superconductivity at 93 K in a New Mixed-Phase Y- Ba-Cu-O Compound System at Ambient Pressure. *Physical Rev. Lett.* 58(198): 908-910.
<http://dx.doi.org/10.1103/PhysRevLett.58.908>
- Yu R, Vilalta GN, Sandiumenge F, Matinez, B, Pinol S, Obradors X.(1997). Growth rate dependence of the critical currents in directionally solidified $\text{YBa}_2\text{Cu}_3\text{O}_7\text{-YBa}_2\text{CuO}_5$ Superconducting Bars. *Physica C*. 290161-169.
[http://dx.doi.org/10.1016/S0921-4534\(97\)01619-5](http://dx.doi.org/10.1016/S0921-4534(97)01619-5)

Full Length Research Paper

Effect of an axial magnetic field on the heat and mass transfer in rotating annulus

Sofiane ABERKANE^{1*}, Malika IHDENE², Mourad MODERES³ and Abderahmane GHEZAL⁴

¹Département Energétique, Faculté des sciences de l'ingénieur, Université M'Hamed Bougara de Boumerdés-35000, Algérie.

²Université de Yahia Farès, Médéa- 26000, Algérie.

³Faculté des hydrocarbures et de la chimie, Université M'Hamed Bougara de Boumerdés-35000, Algérie.

⁴Laboratoire de mécanique des fluides théorique et appliquée, Faculté de physique, Université des sciences et de la technologie de Houari Boumediene Bab Ezzouar, Alger-16111, Algérie.

Received 27 May 2014; Accepted 4 August, 2014

This study is interested in the effect of an axial magnetic field imposed on incompressible flow of electrically conductive fluid between two horizontal coaxial cylinders. The imposed magnetic field is assumed uniform and constant. The effect of heat generation due to viscous dissipation is also taken into account. The inner and outer cylinders are maintained at different uniform temperatures and concentrations. The movement of the fluid is due to rotation of the cylinder with a constant speed. An exact solution of the governing equations for momentum and energy are obtained in the form of Bessel functions. A finite difference implicit scheme was used in the numerical solution to solve the governing equations of convection flow and mass transfer. The velocity, concentration and temperature distributions were obtained with and without the magnetic field. The results show that for different values of the Hartmann number, the velocity and concentration between the two cylinders decreases as the Hartmann number increases. On the other hand, the Hartmann number does not affect the temperature. Also, it is found that by increasing the Hartmann number, the Nusselt and Sherwood numbers decreases.

Key words: Rotating cylinders, viscous dissipation, heat transfer, mass transfer, magnetic field, Bessel function, finite difference.

INTRODUCTION

The study of flow of electrically conductive fluids, called magnetohydrodynamic (MHD) has attracted much attention due to its various applications. In astrophysics and geophysics, it is applied to the study of stellar structures, terrestrial cores and solar plasma. In industrial processes, it finds its application in MHD pumps, nuclear

reactors, the extraction of geothermal energy, metallurgical and crystal growth in the field of semiconductors, the control of the behavior of fluid flow and the stability of convective flows. The analysis of flow and heat and mass transfer, known as the double-diffusive convection, in cylindrical annuli has been

*Corresponding author. E-mail: aberkane.sofian@gmail.com

Author(s) agree that this article remain permanently open access under the terms of the [Creative Commons Attribution License 4.0 International License](https://creativecommons.org/licenses/by/4.0/)

investigated in several pieces of literature. However, to the author's knowledge a few studies have been conducted on double-diffusive convection in a rotating annulus in the presence of a magnetic field. Recently, the effect of magnetic field on the laminar convection in either vertical or horizontal rotating concentric annuli has been investigated. Ben and Henry. (1996) investigated numerically the effect of a constant magnetic field on a three-dimensional buoyancy-induced flow in a cylindrical cavity, they put in light the structural changes of the flow induced by the magnetic field for each field orientation. Singh et al. (1997) presented exact solutions for fully developed natural convection in open-ended vertical concentric annuli under a radial magnetic field. El Amin (2003) studied the effects of both first- and second-order resistance due to the solid matrix on forced convective flow from a horizontal circular cylinder in the presence of a magnetic field and viscous dissipation, with a variable surface temperature boundary condition. Hayat and Kara (2006) investigated the Couette time-dependent flow of an incompressible third-grade fluid subjected to a magnetic field of variable strength analytically. Group theoretic methods were employed to analyze the nonlinear problem and a solution for the velocity field was obtained analytically. Sankar et al. (2006) studied numerically a natural convection of a low Prandtl number electrically conducting fluid under the influence of either axial or radial magnetic field in a vertical cylindrical annulus. They showed that the magnetic field can be suppress the flow and heat transfer. Bessaïh et al. (2009) studied the MHD stability of an axisymmetric rotating flow in a cylindrical enclosure containing liquid metal ($Pr = 0.015$), with an aspect ratio equal to 2, and subjected to a vertical temperature gradient and an axial magnetic field. Azim et al. (2010) studied numerically the effect of magnetic field and Joule heating on the coupling of convection flow along and conduction inside a vertical flat plate in the presence viscous dissipation and heat generation. Ellahi et al. (2010) determined analytic solutions for a nonlinear problem governing the MHD flow of a third grade fluid in the annulus of rotating concentric cylinders. Makinde and Onyejekwe (2011) investigated a steady flow and heat transfer of an electrically conducting fluid with variable viscosity and electrical conductivity between two parallel plates in the presence of a transverse magnetic field. Kakarantzas et al. (2011) studied numerically the combined effect of a horizontal magnetic field and volumetric heating on the natural convection flow and heat transfer of a low Prandtl number fluid in a vertical annulus. Seth et al. (2011) studied the effects of rotation and magnetic field on unsteady Couette flow of a viscous incompressible electrically conducting fluid between two horizontal parallel porous plates in a rotating medium. Mozayyeni and Rahimi (2012) investigated numerically the problem of mixed convection of a fluid in the fully developed region

between two horizontally concentric cylinders with infinite lengths, in the presence of a constant magnetic field with a radial MHD force direction, considering the effects of viscous heat dissipation in the fluid in both steady and unsteady states. Seth and Singh (2013) studied theoretically the effect of Hall current and a uniform transverse magnetic field on unsteady MHD Couette flow of class-II in a rotating system. Takhar et al. (2003) studied the unsteady mixed convection flow over a rotating vertical cone in the presence of a magnetic field. Recently, some attention has been paid by Ashorynejad (2013) to the effect of magnetic field convection on natural convection heat transfer in a horizontal cylindrical annulus enclosure filled with nanofluid using the Lattice Boltzmann method. Also Sheikholeslami et al. (2013) solved the problem of heat and fluid flow of a nanofluid in a half-annulus enclosure with one wall under constant heat flux in presence of magnetic field using control volume based finite element method. In another publication Sheikholeslami et al. (2014) applied Lattice Boltzmann Method to simulate the effect of magnetic field on free convection of nanofluid, in an eccentric semi-annulus. In a recent paper Aminfar et al. (2014) experimentally studied the effects of using magnetic nanofluid and also applying an external magnetic field on the critical heat flux of subcooled flow boiling in vertical annulus.

Some surveyed studies in the literature were concerned primarily with the double diffusive convection, Teamah (2007) carried out a numerical study of double-diffusive laminar mixed convection within a two-dimensional, horizontal annulus rotating cylinders. The results for both average Nusselt and Sherwood numbers were correlated in terms of Lewis number, thermal Rayleigh number and buoyancy ratio. Moreover, Molki et al. (1990) applied the naphthalene sublimation technique to an annulus with a rotating inner cylinder in order to study heat transfer in the entrance region to obtain heat transfer data for laminar flows and compare them with results of mass transfer. Kefeng and Wen-Qiang (2006) simulated numerically the characteristics of transient double-diffusive convection in a vertical cylinder using a finite element method. Recently, Venkatachalappa et al. (2011) carried out numerical computations to investigate the effect of axial or radial magnetic field on the double-diffusive natural convection in a vertical cylindrical annular cavity.

Although the exact solutions for the Hartmann flow and the MHD Couette flow have been achieved for more than seventy years, the solutions for a heat transfer in flow between concentric rotating cylinders, also known as Taylor Couette flows, under external magnetic field have been restricted to high Hartmann numbers.

The aim of the present study is to examine analytically and numerically the effects of an external axial magnetic field applied to the forced convection flow of an electrically conducting fluid between two horizontal

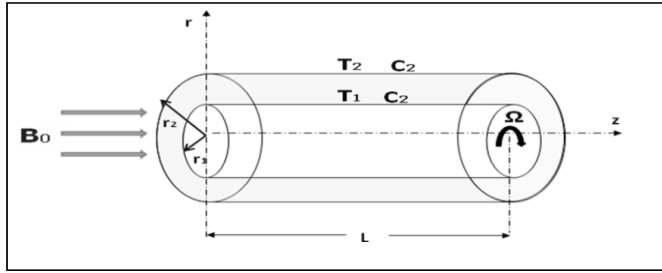


Figure 1. Geometry of the problem.

concentric cylinders, considering the effects of viscous heat dissipation in the fluid. Also we investigated numerically the effects of the magnetic field on the mass transfer in the annular cavity. It should be noted that the natural convection is supposed negligible in this work, which is not always the case of the vertical cylinder. The forced flow is induced by the rotating inner cylinder, in slow constant angular velocity and the other is fixed.

FORMULATION OF THE PROBLEM

Consider a laminar flow of a viscous incompressible electrically conductive fluid between two coaxial cylinders. The inner cylinder of radius r_1 is rotated at a constant speed Ω_1 and the outer cylinder of radius r_2 is kept fixed. The inner and outer walls are maintained at a constant and different temperatures and concentrations, but their values for the inner are higher than the outer, while the top and bottom walls are insulated and impermeable. The two cylinders are electrically isolated. The flow is subjected to a constant uniform and axially magnetic field B_0 . Geometry of the problem is presented in Figure 1. We assume that the magnetic Reynolds number is neglected. When the magnetic field is uniform and externally applied, its time variations can be neglected and the set of flow equations further simplified to involve only the Navier-Stokes equations and the conservation of the electric current. Also we assume that the electric field is zero. In this study the viscous dissipation term in the energy equation is considered.

ANALYTICAL STUDY

The flow is assumed to be steady, laminar and unidirectional, therefore the radial and axial components of the velocity and the derivatives of the velocity with respect to θ and z are zero. Under these assumptions and in cylindrical coordinates, the governing equations for the flow following the azimuthal direction can be written as follows:

$$v \left(\frac{\partial^2 v}{\partial r^2} + \frac{1}{r} \frac{\partial v}{\partial r} - \frac{v}{r^2} \right) - \frac{\sigma v B_0^2}{\rho} = 0 \tag{1}$$

$$\frac{k}{r} \frac{\partial}{\partial r} \left(r \frac{\partial T}{\partial r} \right) = -\mu \left(\frac{\partial v}{\partial r} - \frac{v}{r} \right)^2 \tag{2}$$

$$r = r_1 : v(r) = \Omega_1 r_1, T = T_1 \tag{3}$$

$$r = r_2 : v(r) = \Omega_2 r_2, T = T_2 \tag{4}$$

The governing equation and boundary conditions, Equations (1) to (4), which are in non-adimensional form, become:

$$\frac{\partial^2 v^*}{\partial r^{*2}} + \frac{1}{r^*} \frac{\partial v^*}{\partial r^*} - \left(\frac{Ha^2}{(1-\eta)^2} + \frac{1}{r^{*2}} \right) v^* = 0 \tag{5}$$

$$\frac{1}{r^*} \frac{\partial}{\partial r^*} \left(r^* \frac{\partial \theta}{\partial r^*} \right) = -Ec Pr \left(\frac{\partial v^*}{\partial r^*} - \frac{v^*}{r^*} \right)^2 \tag{6}$$

$$r^* = \eta : v^*(r^*) = 1, \theta = 1 \tag{7}$$

$$r^* = 1 : v^*(r^*) = b, \theta = 0 \tag{8}$$

Where

$$r^* = \frac{r}{r_2}, v^* = \frac{v}{\Omega_1 r_1}, \eta = \frac{r_1}{r_2}, b = \frac{\Omega_2 r_2}{\Omega_1 r_1}, Ha = B_0 d \sqrt{\frac{\sigma}{\rho \nu}}, \theta = \frac{T - T_2}{T_1 - T_2}, Pr = \frac{\nu}{a}, Ec = \frac{(\Omega_1 r_1)^2}{C_p \Delta T}$$

Where, the stars are dropped for convenience. The velocity profile in the annular space is obtained by solving the Equation (5) as follows:

$$v(r) = C_1 I_1 \left(\frac{Ha}{1-\eta} r \right) + C_2 K_1 \left(\frac{Ha}{1-\eta} r \right) = 0 \tag{9}$$

Where:

$$M = \frac{Ha}{1-\eta}$$

C_1 and C_2 are the constants of integration, which are determined from the boundary conditions on the velocity.

$$C_1 = \frac{K_1(M) - b K_1(\eta M)}{I_1(\eta M) K_1(M) - K_1(\eta M) I_1(M)}$$

$$C_2 = \frac{b I_1(\eta M) - I_1(M)}{I_1(\eta M) K_1(M) - K_1(\eta M) I_1(M)}$$

I_1 is the modified Bessel function of the first kind of order 1, and K_1 is the modified Bessel function of the second kind of order 1. To obtain the temperature field from Equation (6), we performed calculations by using the expansions with three terms of the modified Bessel functions $I_1(Mr)$ and $K_1(Mr)$ used by Omid et al. (2012), for small values of Ha . It can be used as following:

$$I_1(Mr) \cong \frac{1}{2}Mr + \frac{(Mr)^3}{16} + \frac{(Mr)^5}{384} \tag{10}$$

$$K_1(Mr) \cong \frac{1}{Mr} + \left[\frac{1}{2} \ln\left(\frac{Mr}{2}\right) - \frac{1}{4}(-2\gamma + 1) \right] (Mr) + \left[\frac{1}{16} \ln\left(\frac{Mr}{2}\right) - \frac{1}{32}\left(\frac{5}{2} - 2\gamma\right) \right] (Mr)^3 \tag{11}$$

Where γ is Euler's constant defined by:

$$\gamma = \lim_{x \rightarrow \infty} \left[1 + \frac{1}{2} + \frac{1}{3} + \frac{1}{4} + \dots + \frac{1}{m} - \ln(m) \right] = 0,5772156649\dots$$

By substituting the values of $I_1(Mr)$ and $K_1(Mr)$ from the above expansions in the velocity equation, Equation (9), and using the new velocity distribution in Equation (6) to find the temperature field. The temperature gradient is given then by the following equation:

$$\frac{\partial \theta}{\partial r} = \frac{C_3}{r} - \frac{Br}{r} + \left[\begin{aligned} &2C_2^2 \ln\left(\frac{Mr}{2}\right) + \frac{2C_2^2}{Mr^2} + C_5(Mr)^6 \ln\left(\frac{Mr}{2}\right) + \\ &C_6(Mr)^6 - \frac{1}{384}C_2^2(Mr)^6 \left(\ln\left(\frac{Mr}{2}\right) \right)^2 \\ &+ C_7(Mr)^2 + C_8(Mr)^4 - \frac{1}{32}C_2^2(Mr)^4 \ln\left(\frac{Mr}{2}\right) \\ &+ C_9(Mr)^8 - \frac{1}{3072}C_1C_2(Mr)^8 \ln\left(\frac{Mr}{2}\right) \\ &-\frac{1}{92160}C_1^2(Mr)^{10} \end{aligned} \right] \tag{12}$$

Where the constants C_5 to C_9 are given in terms of C_1 and C_2 as follows:

$$C_5 = \frac{11}{2304}C_1^2 - \frac{1}{192}C_1C_2 - \frac{1}{192}C_2^2\gamma$$

$$C_6 = \frac{11}{2304}C_2^2\gamma + \frac{7}{2304}C_1C_2 - \frac{1}{384}C_2^2\gamma - \frac{1}{384}C_1^2 - \frac{125}{55296}C_2^2 - \frac{1}{192}C_1C_2\gamma$$

$$C_7 = \frac{1}{4}C_2^2\gamma - \frac{7}{16}C_2^2 + \frac{1}{4}C_1C_2$$

$$C_8 = \frac{1}{32}C_2^2 - \frac{1}{32}C_2^2\gamma - \frac{1}{48}C_1C_2$$

$$C_9 = \frac{7}{24576}C_1C_2 - \frac{1}{3072}C_1C_2\gamma - \frac{1}{3072}C_1^2$$

The solution of the energy equation is:

$$\theta = C_4 + C_3 \ln(r) + Br \left[\begin{aligned} &C_{10}(Mr)^6 + C_{11}(Mr)^8 + C_{12}(Mr)^4 + \frac{1}{2}C_7(Mr)^2 - \frac{1}{92160}C_1^2(Mr)^{10} \\ &+ C_2^2 \left(\ln\left(\frac{Mr}{2}\right) \right)^2 + 2C_2^2 \ln\left(\frac{Mr}{2}\right) + \frac{C_2^2}{(Mr)^2} + \frac{1}{6}C_5(Mr)^6 \ln\left(\frac{Mr}{2}\right) \\ &+ C_6(Mr)^6 - \frac{1}{2304}C_2^2(Mr)^6 \left(\ln\left(\frac{Mr}{2}\right) \right)^2 + \frac{1}{6912}C_2^2(Mr)^6 \ln\left(\frac{Mr}{2}\right) \\ &-\frac{1}{128}C_2^2(Mr)^4 \ln\left(\frac{Mr}{2}\right) - \frac{1}{24576}C_1C_2(Mr)^8 \ln\left(\frac{Mr}{2}\right) \end{aligned} \right] \tag{13}$$

Where the Constants C_{10} , C_{11} and C_{12} are given as follows:

$$C_{10} = \frac{1}{36}C_5 + \frac{1}{6}C_6 - \frac{1}{41472}C_2^2$$

$$C_{11} = \frac{1}{8}C_9 + \frac{1}{196608}C_1C_2$$

$$C_{12} = \frac{1}{4}C_8 + \frac{1}{512}C_2^2$$

NUMERICAL STUDY

In this numerical study, we consider two-dimensional and axisymmetric unsteady flow. We opted for the velocity - pressure formulation due to its rapidity of prediction, its lower cost, and its ability to simulate real conditions. The finite difference scheme adopted for the resolution is very similar to that used by Peyrret (1976), and Ghezal and Porterie. (2011), this is a semi implicit scheme of Crank-Nicholson type, iterative process based on the perturbation of the continuity equation by introducing an artificial compressibility. The spatial discretization using the marker and cell (MAC) is shown in Figure 2. The iterative procedure is assumed converged when the following test is verified

$$\max(|L_u|, |L_v|, |L_w|, |L_\theta|, |L_C| |D|) < \epsilon$$

where L_u , L_v , L_w , L_θ , L_C and D represents operators differences relating to system equations corresponding to the problem variables u , v , w , θ , C and Π respectively, ϵ is of the order of 10^{-5} depending on the considered case.

We then proceeded to a study of the mesh sensitivity of the field of study. This study led us to retain a mesh of 336 nodes along the direction r and 48 nodes in the z direction.

Mathematical equations

Based on these dimensionless variables, the conservation equations of mass, momentum and energy are written in non rotating frame cylindrical coordinates as follows (where the stars are dropped for convenience):

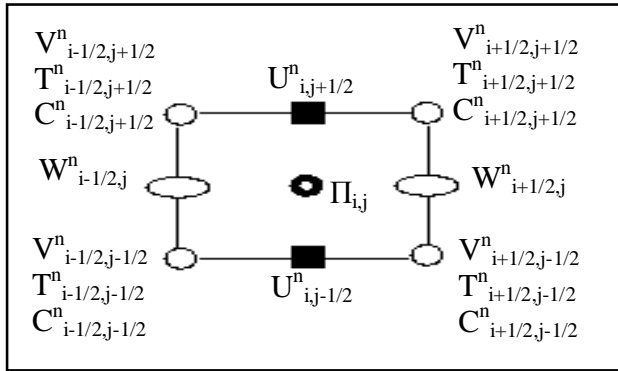


Figure 2. M.A.C cell.

$$\frac{\partial \mathbf{u}}{\partial \mathbf{r}} + \frac{\mathbf{u}}{\mathbf{r}} + \frac{\partial \mathbf{w}}{\partial \mathbf{z}} = 0 \tag{14}$$

$$\frac{\partial u}{\partial t} + u \frac{\partial u}{\partial r} + \frac{v^2}{r} + w \frac{\partial u}{\partial z} = -\frac{\partial \Pi}{\partial r} + \frac{1-\eta}{\text{Ta}} \left(\frac{\partial^2 u}{\partial r^2} + \frac{1}{r} \frac{\partial u}{\partial r} + \frac{\partial^2 u}{\partial z^2} - \frac{u}{r^2} \right) - \frac{\text{Ha}^2 u}{(1-\eta)\text{Ta}} \tag{15}$$

$$\frac{\partial v}{\partial t} + u \frac{\partial v}{\partial r} + \frac{vu}{r} + w \frac{\partial v}{\partial z} = \frac{1-\eta}{\text{Ta}} \left(\frac{\partial^2 v}{\partial r^2} + \frac{1}{r} \frac{\partial v}{\partial r} + \frac{\partial^2 v}{\partial z^2} - \frac{v}{r^2} \right) - \frac{\text{Ha}^2 v}{(1-\eta)\text{Ta}} \tag{16}$$

$$\frac{\partial w}{\partial t} + u \frac{\partial w}{\partial r} + w \frac{\partial w}{\partial z} = -\frac{\partial \Pi}{\partial z} + \frac{1-\eta}{\text{Ta}} \left(\frac{\partial^2 w}{\partial r^2} + \frac{1}{r} \frac{\partial w}{\partial r} + \frac{\partial^2 w}{\partial z^2} \right) \tag{17}$$

$$\frac{\partial \theta}{\partial t} + u \frac{\partial \theta}{\partial r} + w \frac{\partial \theta}{\partial z} = \frac{1-\eta}{\text{PrTa}} \left(\frac{\partial^2 \theta}{\partial r^2} + \frac{1}{r} \frac{\partial \theta}{\partial r} + \frac{\partial^2 \theta}{\partial z^2} \right) + \frac{(1-\eta)\text{Ec}\Phi}{\text{Ta}} \tag{18}$$

$$\frac{\partial C}{\partial t} + u \frac{\partial C}{\partial r} + w \frac{\partial C}{\partial z} = \frac{1-\eta}{\text{ScTa}} \left(\frac{\partial^2 C}{\partial r^2} + \frac{1}{r} \frac{\partial C}{\partial r} + \frac{\partial^2 C}{\partial z^2} \right) \tag{19}$$

Where:

$\text{Ha} = \text{Bd} \sqrt{\frac{\sigma}{\rho \nu}}$ is the Hartmann number,

$\text{Ta} = \frac{\Omega_1 r_1 d}{\nu}$ is the Taylor number,

$\text{Pr} = \frac{\nu}{a}$ is the Prandtl number

$\text{Sc} = \frac{\nu}{D}$ is the Schmidt number,

$d = r_1 - r_2$ is the width of the annular space,

$\Phi = 2 \left[\left(\frac{\partial u}{\partial r} \right)^2 + \left(\frac{u}{r} \right)^2 + \left(\frac{\partial w}{\partial z} \right)^2 \right] + \left(\frac{\partial u}{\partial z} + \frac{\partial w}{\partial r} \right)^2 + \left(\frac{\partial v}{\partial r} - \frac{v}{r} \right)^2 + \left(\frac{\partial v}{\partial z} \right)^2$ is the viscous dissipation function.

The rate of heat transfer in non – dimensional for the inner and outer cylinder is given by:

$$\text{Nu}_i(z) = -\xi \frac{\partial \theta}{\partial r} \Big|_{r=\eta}$$

$$\text{Nu}_e(z) = -\xi \frac{\partial \theta}{\partial r} \Big|_{r=1}$$

With: $\xi = 1 - \eta$

The average Nusselt number on the inner and outer cylinders is given by:

$$\overline{\text{Nu}}_i = \frac{1}{L} \int_0^z \text{Nu}_i(z) dz$$

$$\overline{\text{Nu}}_e = \frac{1}{L} \int_0^z \text{Nu}_e(z) dz$$

Similarly, we can calculate both local Sherwood number as follows:

$$\text{Sh}_i(z) = -\xi \frac{\partial C}{\partial r} \Big|_{r=\eta}$$

$$\text{Sh}_e(z) = -\xi \frac{\partial C}{\partial r} \Big|_{r=1}$$

Initial and boundary conditions

At the time $t=0$:

$$u(r, z, 0) = v(r, z, 0) = w(r, z, 0) = \Pi(r, z, 0) = \theta(r, z, 0) = C(r, z, 0) = 0 \tag{20}$$

The boundary conditions are as follows:

$$r = \eta \quad z \geq 0 : u(r_1, z) = v(r_1, z) = w(r_1, z) = 0$$

$$\theta(r_1, z) = C(r_1, z) = 1 \tag{21}$$

$$r = 1 \quad z \geq 0 : u(r_2, z) = v(r_2, z) = w(r_2, z) = 0$$

$$\theta(r_2, z) = C(r_2, z) = 0 \tag{22}$$

$$\eta < r < 1 \quad z = 0 : u = v = w = 0, \frac{\partial C}{\partial z} = \frac{\partial \theta}{\partial z} = 0 \tag{23}$$

$$z = L : u = v = w = 0, \frac{\partial \theta}{\partial z} = \frac{\partial C}{\partial z} = 0 \tag{24}$$

RESULTS AND DISCUSSION

In order to understand the physical situation of the problem and the effects of the Hartmann and Eckert numbers, we have found the numerical and analytical

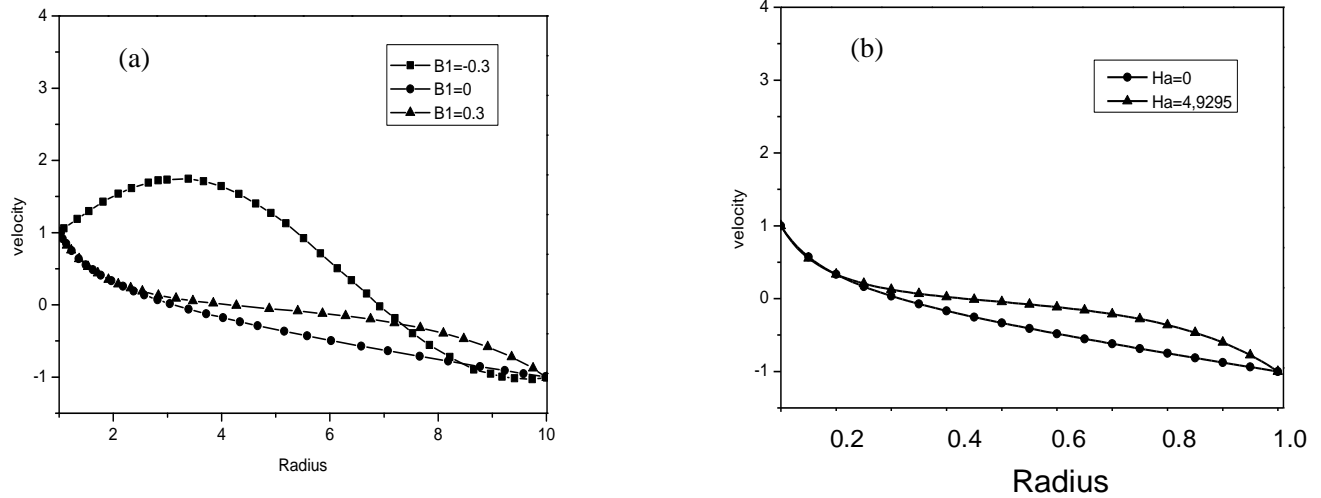


Figure 3. Velocity profile of the fluid in the annulus for $b = -1$, (a) Result of Dizaji Feiz et al. (2008), (b) Results of the present analytical study.

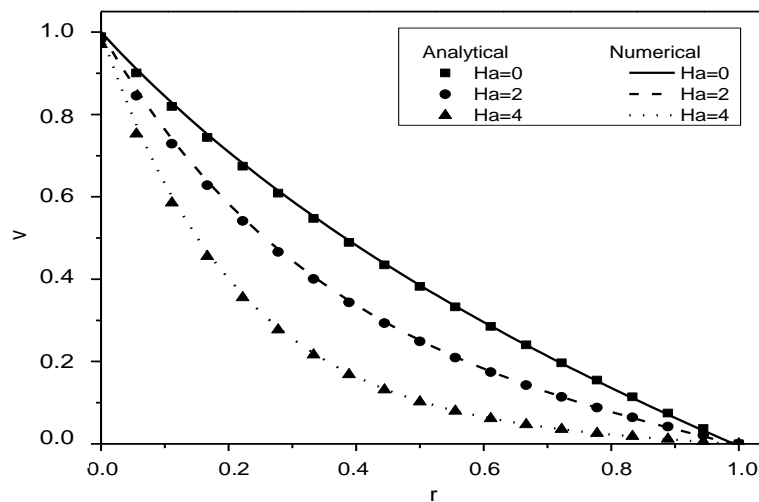


Figure 4. Comparison of analytical and numerical results of velocity profile, for $\eta = 0.5, b = 0, Ta = 20, t^* = 120$.

values of the velocity, temperature, concentration, the Nusselt number and Sherwood number. The analytical method developed in the present work has been compared in Figure 3 with the results obtained by Feiz-Dizaji (2008), for the velocity profiles of the fluid in the annulus of concentric cylinders with velocity ratio $b = -1$. The results are found to be in good agreement except for the negative values of magnetic field B_1 which cannot exist in our non-dimensional study, Hartmann number (Ha) is a strictly positive non-dimensional number.

The results obtained through the developed code in FORTRAN based on an implicit finite-difference method

described earlier, are compared with those calculated using the analytical approach for small value of Hartmann number. The velocity, temperature and average Nusselt numbers are evaluated analytically and numerically for different values of Hartmann number in Figures 4, 5 and 6.

Obviously, the velocity and temperature profiles, for various Ha obtained via these two different methods, agree with each other reasonably well. We can notice in Figure 4 that the velocity profile without magnetic field $Ha = 0$ is quasi-linear, and an increase in Hartman number, which causes a reduction of the velocity in the annular space because the centrifugal force is counter-productive

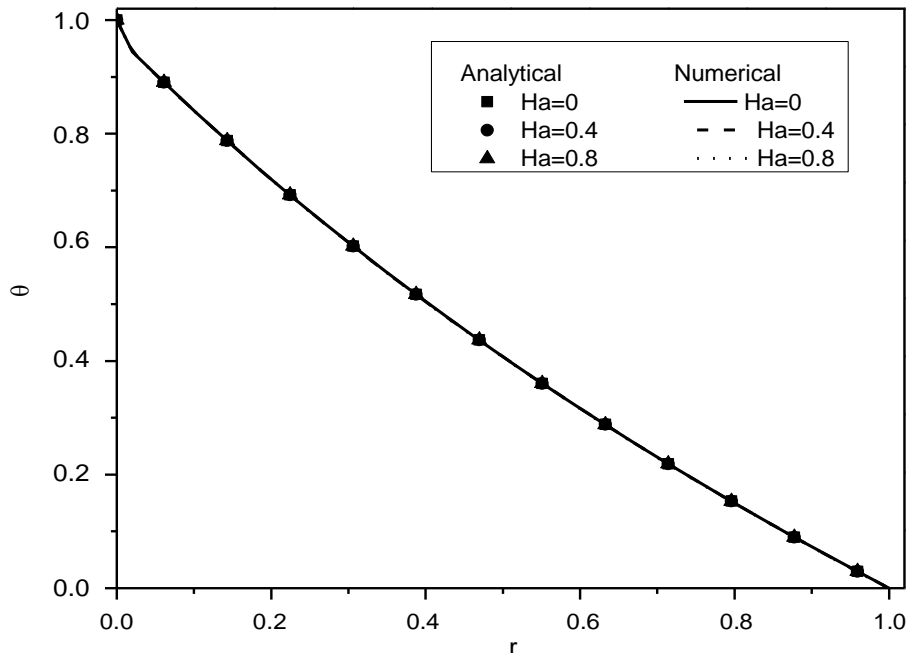


Figure 5. Comparison of analytical and numerical results of temperature profile, for $\eta = 0.5, b=0, Ta=20, Pr = 0.02, Ec=0.5, t=120$.

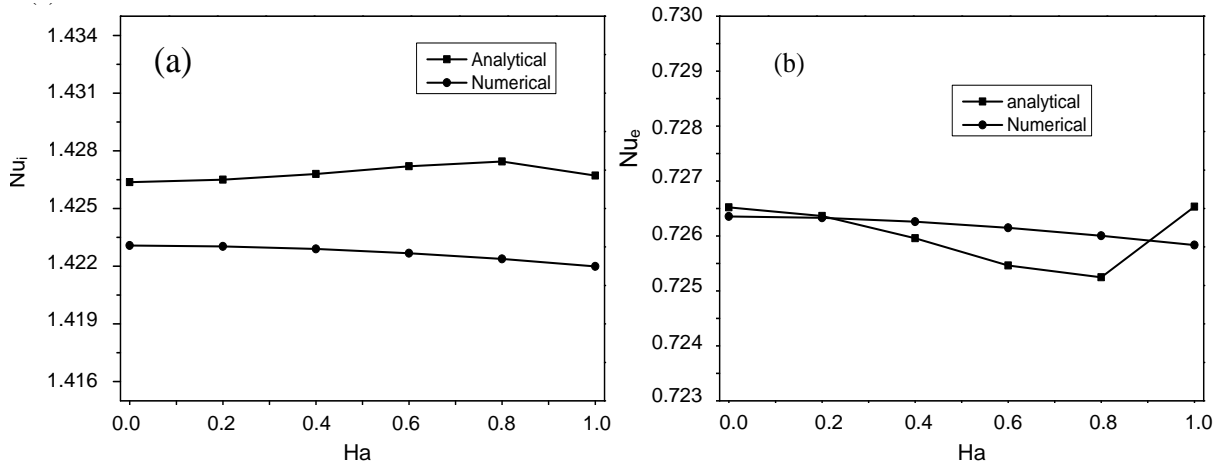


Figure 6. Comparison of analytical and numerical results of average Nusselt number on (a) inner and (b) outer surfaces of the cylinder against the Hartmann number, for $\eta = 0.5, b=0, Pr = 0.02, Ec=0.5$.

and the Lorentz electromagnetic force acts as a flow damper. It is observed from Figure 5 that the effect of weak magnetic field on the radial profile of temperature is insignificant for small value of Prandtl numbers ($Pr=0.02$) which is appropriate for liquid metal. It is valid in the case of low and high values of Hartmann number. Figure 6 displays the effect of Hartmann number on the average Nusselt number on inner and outer surfaces. As can be seen, from this figure that the analytic approach

corresponding to the expansion with three terms of the modified Bessel functions is closer to the numerical approach. The difference between the analytical and numerical values is approximately 10^{-3} , even the results obtained from the present theoretical analysis are restricted to a one-dimensional flow and the numerical results are calculated using two-dimensional axisymmetric flow. Figure 7 shows the effect of Hartmann number on the local Nusselt number on the inner and

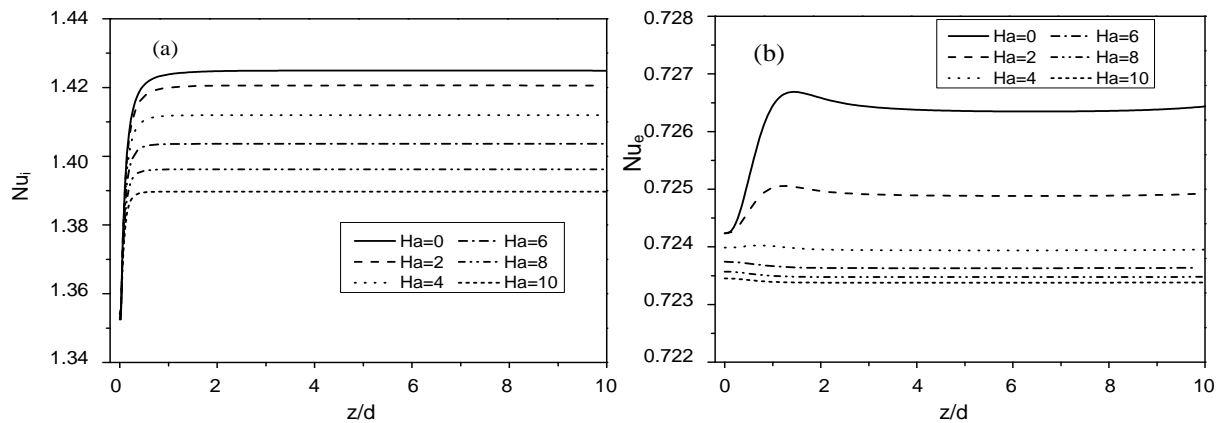


Figure 7. Effect of Hartman number on local Nusselt number distribution on (a) inner and (b) outer cylinders, for $\eta = 0.5$, $Pr = 0.02$, $Ec = 0.5$, $t^* = 120$.

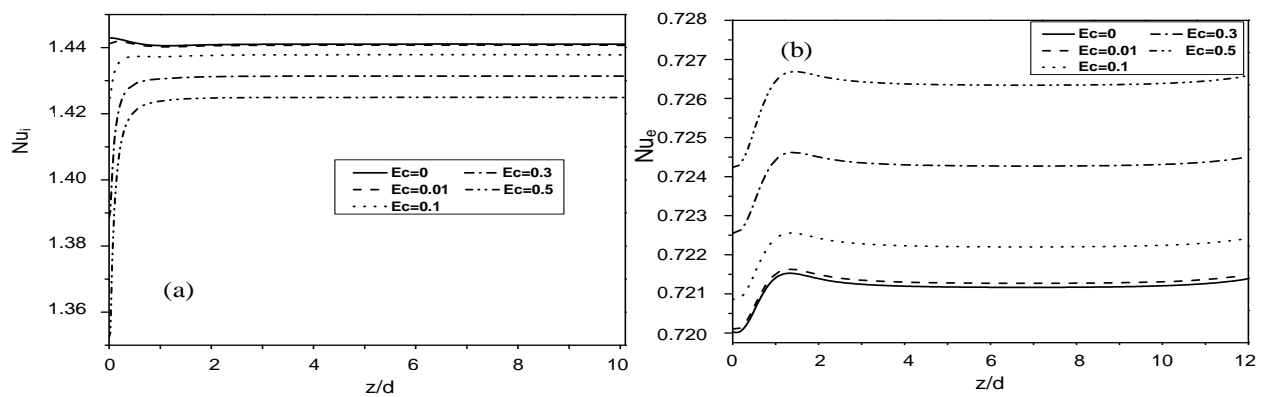


Figure 8. Effect of Eckert number on local Nusselt number distribution on (a) inner and (b) outer cylinders, for $\eta = 0.5$, $Pr = 0.02$, $Ha = 0$, $t^* = 120$.

outer surfaces, for an Eckert number $Ec = 0.5$. It is found that for high values of Hartmann number, the local Nusselt number on the inner and outer surfaces decreases.

In fact when the Eckert number is considerable, the heat generation in the fluid increases because of the viscous dissipation. Thus the temperature of the fluid in the annular space increases causing a decrease in the temperature gradient in the vicinity of the inner cylinder and an increase of the gradient in the vicinity of the outer cylinder. A significant increase in the Hartmann number causes a reduction of the centrifugal force, which results in a gradual decrease in the Nusselt number. It is worth to mention that this phenomenon is in full accordance with what was previously observed by Mozayyeni (2013) for a horizontal cylindrical annulus, also by El-Amin (2003) for horizontal cylinder in a porous medium and by Takhar et al. (2003). for rotating vertical cone.

The analysis of the variation of local Nusselt number on the inner and outer cylinder shows that this number tends to a limit value. It can be noticed that the Nusselt number on the outer cylinder is lower than on the inner cylinder, because the velocity and temperature gradient are higher for the cold inner cylinder than for the outer cylinder. It should be also noted that the effect of magnetic field on the temperature distribution is insignificant, whereas the changes induced by the magnetic field on the temperature gradient and therefore on the Nusselt number is considerable.

Effect of Eckert number on the distribution of local Nusselt number on the inner and outer cylinders is displayed in Figure 8, for $Ha = 0$. As can be seen, with increase of Eckert number, the influence of heat transfer due to the viscous dissipation in the annular space is improved, which leads to the increase in the average temperature of the fluid at this region, especially near the

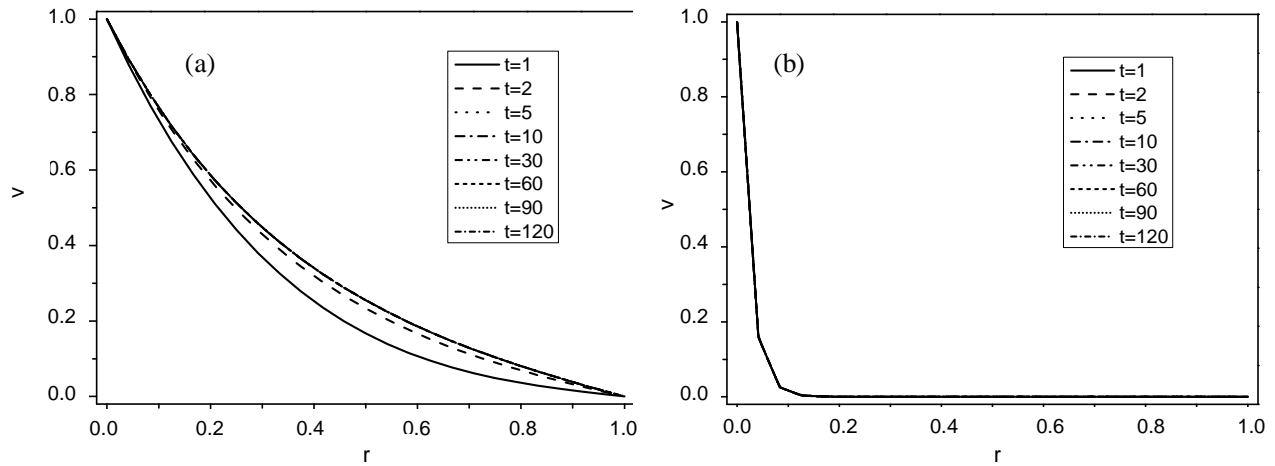


Figure 9. Velocity distribution at different times at $z/d=7$ and for $Ta=20$, (a) $Ha = 2$ and (b) $Ha = 50$.

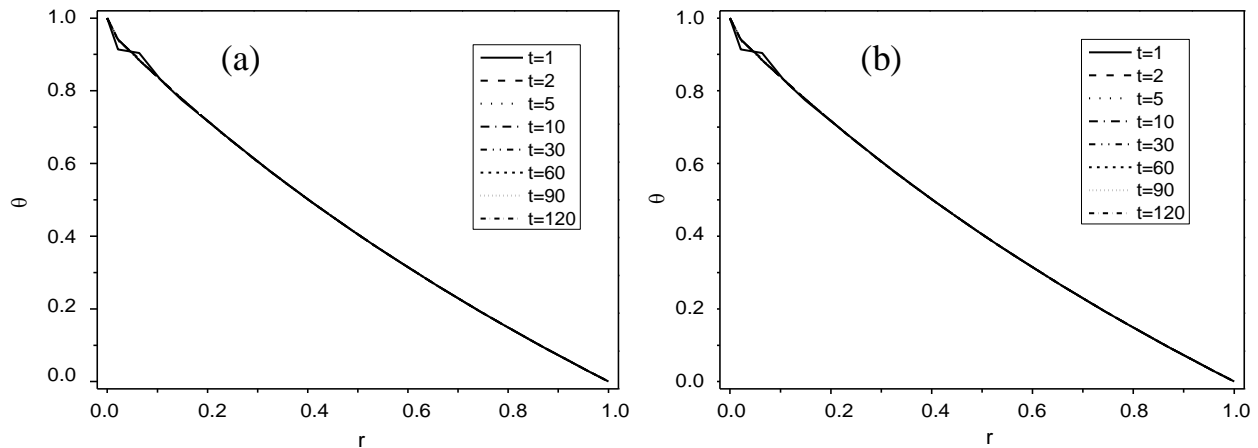


Figure 10. Temperature distribution at different times for $z/d=7$, $Ta=20$, $Ec=0$, $Pr=0.02$, for (a) $Ha = 2$ and (b) $Ha=50$.

inner cylinder, to be more than in the past. The dimensionless temperatures of inner and outer cylinders are maintained at 1.0 and 0.0, respectively.

It is evident that by increasing the average temperature of fluid in annular space, the rate of heat transfer between the fluid and inner cylinder decreases due to the reduction of the temperature difference between them. In contrast to the other case, the local Nusselt number on the outer cylinder increases as the Eckert number increases because of the enhancement of temperature differences between the fluid and the outer cylinder.

In this part, some results are presented in different non-dimensional time values for the distribution of velocity and temperature in the annulus Figures 9, 10, and 11. From Figure 10, we can notice that for a small value of

Prandtl number ($Pr=0,02$), The effect of the time variation is found to be not significant on the temperature, it reaches faster a steady-state to the point that we can't notice the difference between the steady and unsteady states flows. As we know, for larger fluid Prandtl number, the momentum flow transfer is faster than heat transfer. This can be seen clearly in Figure 11 (for a fluid with $Pr =7$) and the distribution of the azimuthal component of velocity reaching a steady-state quicker than the temperature at the mid-length. There is not much difference in velocity at $t= 10$, compared to $t=120$, but comparing temperature distribution at $t=10$ with values greater than 10, it indicates that much more time is still needed to reach steady-state.

The effects of Hartmann number on the concentration

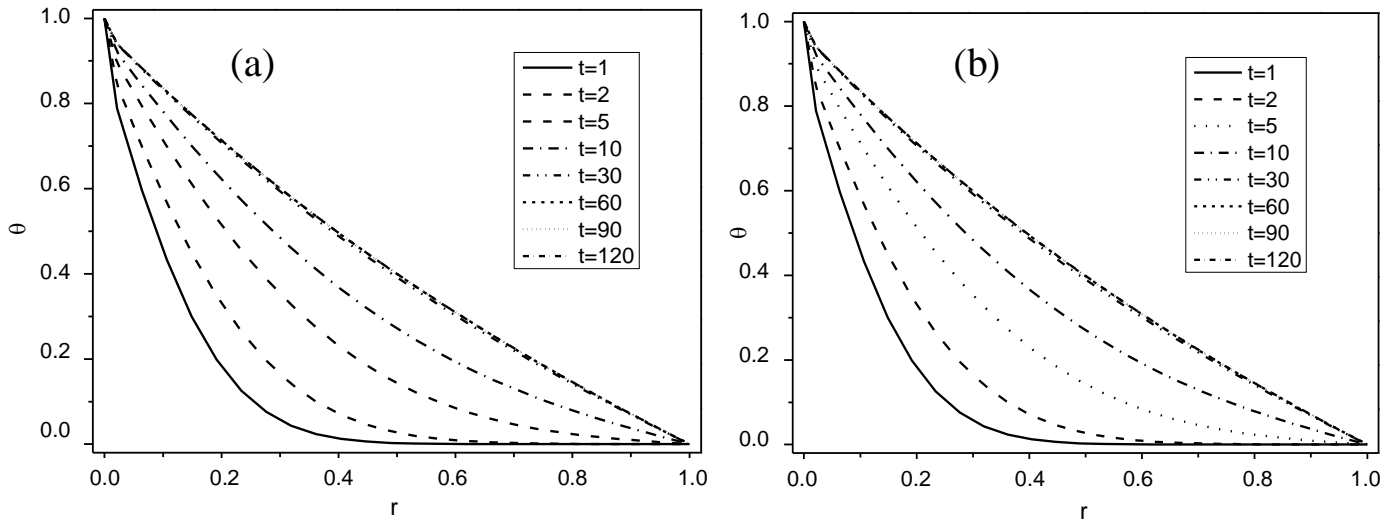


Figure 11. Temperature distribution at different times at $z/d=7$, for $Ta=20$, $Ec=0$, $Pr=7$, for (a) $Ha = 2$ and (b) $Ha = 5$.

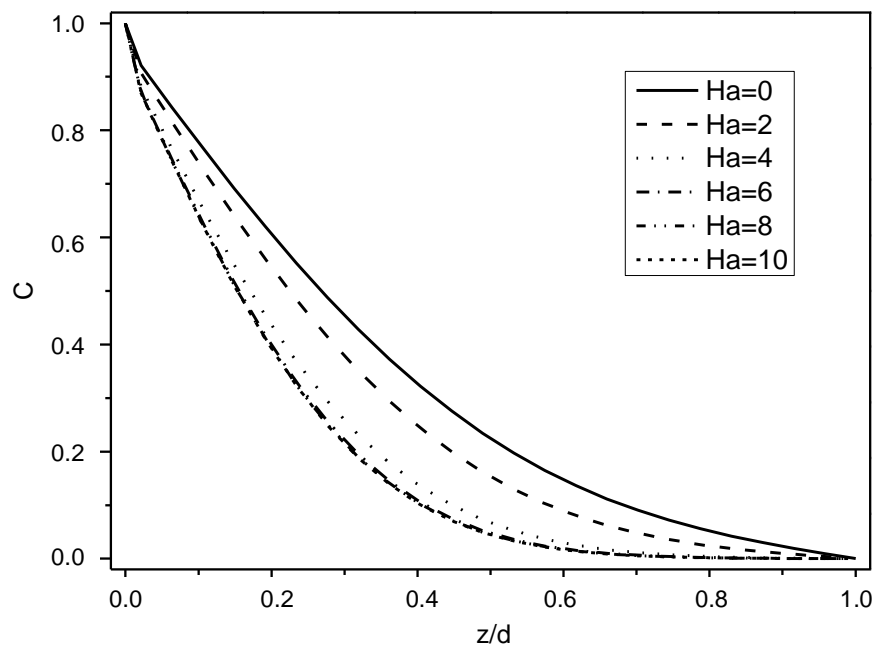


Figure 12. Concentration profile as a function of Hartmann number, for $\eta = 0.5$, $Ta=20$, $Pr= 0.02$, $Ec=0$, $t=120$, $z/d=7$.

At the annulus center are shown in Figure 12. It is observed that the concentration decrease from the inner cylinder where is considered to be a source for the concentration to tends towards almost zero value in the outer cylinder. As can be also seen from this figure, for increasing Hartmann number the concentration decreases in the annular cavity.

The mass transfer rate across the annular cavity is investigated using the computed local Sherwood numbers in the inner and outer cylinders, for different Hartmann number and $Sc=10$ in Figure 13. It can be noticed that the rate of mass transfer is higher on the inner cylinder than on the outer cylinder. This is reasonable to expect since the velocity and concentration

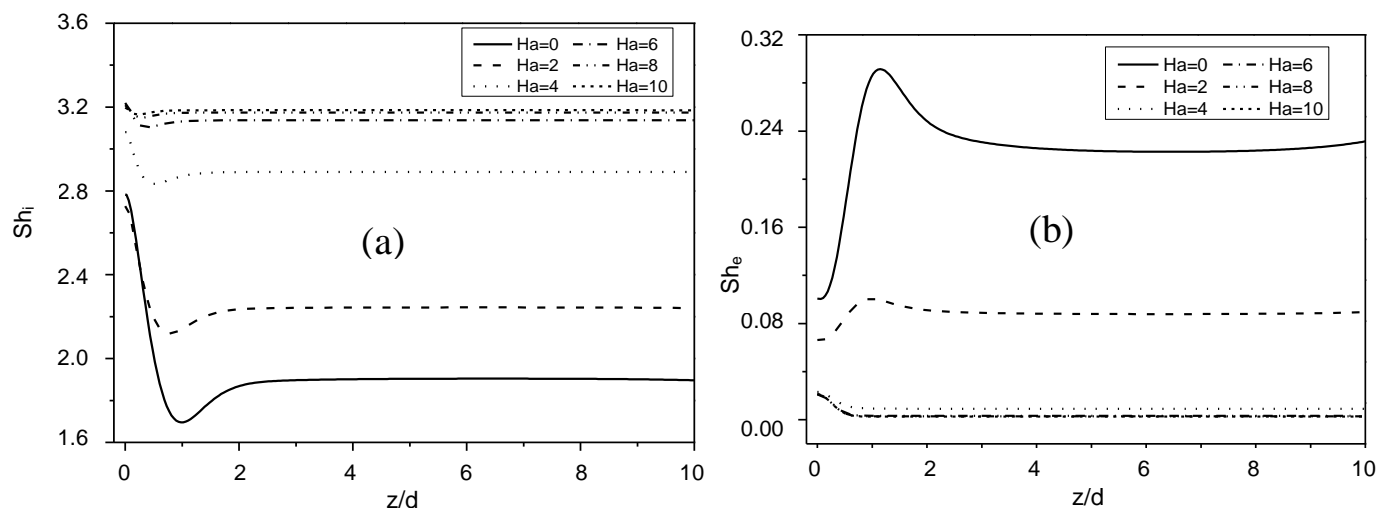


Figure 13. Effect of Hartman number on local Sherwood number distribution on (a) inner and (b) outer cylinders, for $\eta = 0.5$, $Sc=10$, $Ec=0$, $t=120$.

gradient are higher for the inner cylinder than for the outer cylinder. The rate of mass transfer profile on the outer surface is decreased with decreasing the values of the magnetic field parameter. Another interesting point is the unexpected behavior of local Schmidt number with an increase in Hartman number, the application of an axial magnetic field tends to decrease the mass transfer on the inner cylinder.

CONCLUSION

In this study, the MHD forced convection flow and mass transfer of an electrically conducting fluid between two horizontal concentric cylinders in the presence of an axial magnetic field considering the effects of viscous heat dissipation in the fluid has been investigated numerically and analytically. The velocity distribution in the annulus is obtained analytically in terms of the modified Bessel functions whose argument contains Hartmann number and radial coordinate. To obtain the temperature, the expansions of the modified Bessel functions, with three terms are used in the energy equation.

It is found that the velocity and concentration decreases in the annulus with increase of Hartmann number. However, an increase in Hartmann number does not affect the temperature. The effects of magnetic field strength and Eckert number on local Nusselt number have been examined. The results show that an increase in Hartmann number reduces the Nusselt number on both surfaces of the cylinders. Also it was noticed that as the Eckert number increases local Nusselt number increases on the outer cylinder, but opposite trend is observed on the inner cylinder. The application of a magnetic field generates some interesting changes in mass transfer, an

increasing in Hartmann number causes a reduction on the locale Sherwood number.


Conflict of Interest

The authors have not declared any conflict of interest.

REFERENCES

- Aminfar H, Mohammadpourfard M, Maroofiazar R (2014). Experimental study on the effect of magnetic field on critical heat Flux of ferrofluid flow boiling in a vertical annulus. *Exper. thermal. fluid sci.* [:http://dx.doi.org/10.1016/j.exptthermflusci.2014.06.023](http://dx.doi.org/10.1016/j.exptthermflusci.2014.06.023).
- Ashorynejad Hamid RA, Mohamad A, Sheikholeslami M (2013). Magnetic field effects on natural convection flow of a nanofluid in a horizontal cylindrical annulus using Lattice Boltzmann method. *Int. J. Thermal Sci.* pp. 240-250. <http://dx.doi.org/10.1016/j.ijthermalsci.2012.08.006>
- Azim MA, Mamun AA, Rahman MM (2010). Viscous Joule heating MHD-conjugate heat transfer for a vertical flat plate in the presence of heat generation. *Int. Commun. Heat Mass Transfer* 37:666–67. <http://dx.doi.org/10.1016/j.icheatmasstransfer.2010.02.002>
- Ben HH, Henry D (1996). Numerical simulation of convective three-dimensional flows in a horizontal cylinder under the action of a constant magnetic field. *J. Cryst. Growth* 166:436-673. [http://dx.doi.org/10.1016/0022-0248\(96\)00044-9](http://dx.doi.org/10.1016/0022-0248(96)00044-9)
- Bessai R, Boukhari A, Marty PH (2009). Magnetohydrodynamics stability of a rotating flow with heat transfer. *Int. Commun. Heat. Mass Transfer* 36:893-901. <http://dx.doi.org/10.1016/j.icheatmasstransfer.2009.06.009>
- Hayat T, Kara AH (2006). Couette flow of a third-grade fluid with variable magnetic field. *Math. Compute. Modeling* 43:132–137. <http://dx.doi.org/10.1016/j.mcm.2004.12.009>
- EI-Amin MF (2003). Combined effect of viscous dissipation and joule heating on MHD forced convection over a non-isothermal horizontal cylinder embedded in a fluid saturated porous medium. *J. Magnet. Magnetic Mater.* 263:337–343. [http://dx.doi.org/10.1016/S0304-8853\(03\)00109-4](http://dx.doi.org/10.1016/S0304-8853(03)00109-4).
- Ellahi R, Hayat T, Mahomed FM, Zeeshan A (2010). Analytic solutions

- for MHD flow in an annulus. *Commun. Nonlinear. Sci. Numer. Simulat.* 15:1224–1227. <http://dx.doi.org/10.1016/j.cnsns.2009.05.050>
- Feiz-Dizaji A, Salimpour MR, Jam F (2008). Flow field of a third-grade non-Newtonian fluid in the annulus of rotating concentric cylinders in the presence of magnetic field. *J. Math. Anal. Appl.* 337:32–645. <http://dx.doi.org/10.1016/j.jmaa.2007.03.110>.
- Ghezal A, Porterie B (2011). Loraud J.C., Etude dynamique et thermique d'un écoulement pulsé en présence d'un solide chauffé en rotation. *Mécanique Industries* 12:45-65. <http://dx.doi.org/10.1051/meca/2011004>
- Molki M, Astill KN, Leal E (1990). Convective heat-mass transfer in the Convective heat-mass transfer in the entrance region of a concentric annulus having a rotating inner cylinder entrance. *Int. J. Heat. Fluid Flow*, 11:2. [http://dx.doi.org/10.1016/0142-727X\(90\)90005-V](http://dx.doi.org/10.1016/0142-727X(90)90005-V).
- Kakarantzas SC, Sarris IE, Vlachos NS (2011). Natural convection of liquid metal in a vertical annulus with lateral and volumetric heating in the presence of a horizontal magnetic field. *Int. J. Heat. Mass Transfer* 54:3347-3356. <http://dx.doi.org/10.1016/j.ijheatmasstransfer.2011.03.051>
- Makinde OD, Onyejekwe OO (2011). A numerical study of MHD generalized Couette flow and heat transfer with variable viscosity and electrical conductivity. *J. Mag. Magn. Mater.* 323:2757–2763. <http://dx.doi.org/10.1016/j.jmmm.2011.05.040>
- Mozayyeni HR, Rahimi AB (2012). Mixed convection in cylindrical annulus with rotating outer cylinder and constant magnetic field with an effect in the radial direction. *Scientia Iranica B* 19(1)91–105. <http://dx.doi.org/10.1016/j.scient.2011.12.006>
- Omid M, Shohel M, Ioan P (2012). Analysis of first and second laws of thermodynamics between two isothermal cylinders with relative rotation in the presence of MHD flow. *Int. J. Heat Mass Transfer* 55:4808–4816. <http://dx.doi.org/10.1016/j.ijheatmasstransfer.2012.04.048>
- Peyrret R (1976). Unsteady evolution of horizontal jet in a stratified fluid. *J. Fluid mech.* 78:(1):49-63. <http://dx.doi.org/10.1017/S0022112076002322>
- Sankar M, Venkatachalappa M, Shivakumara IS (2006). Effect of magnetic field on natural convection in a vertical cylindrical annulus. *International J. Eng. Sci.* 44:1556–1570. <http://dx.doi.org/10.1016/j.ijengsci.2006.06.004>
- Seth GS, Ansari MdS, Nandkeolyar R (2011). Effects of rotation and magnetic field on unsteady Couette flow in a porous channel. *J. Appl. Fluid Mech.* 4(2):95-103. Available online at www.jafmonline.net
- Seth GS, Singh JK (2013). Effects of Hall current of unsteady MHD Couette flow of class-II in a rotating system. *J. Appl. Fluid Mech.* 6(4):473-484. Available online at www.jafmonline.net
- Sheikholeslami M, Gorji-Bandpy M, Ganji DD, Soleimani S (2013). Effect of a magnetic field on natural convection in an inclined half-annulus enclosure filled with Cu–water nanofluid using CVFEM. *Advan. Powder Technol.* 24(6):980–991. <http://dx.doi.org/10.1016/j.apt.2013.01.012>
- Sheikholeslami M, Gorji-Bandpy M, Ganji DD (2014). MHD free convection in an eccentric semi-annulus filled with nanofluid. *J.Taiwan Instit. Chem. Eng.* 1204–1216. <http://dx.doi.org/10.1016/j.jtice.2014.03.010>.
- Singh SK, Jha BK, Singh AK (1997). Natural convection in vertical concentric annuli under a radial magnetic field. *Heat. Mass Transfer*, 32:399–401, Springer-Verlag. <http://dx.doi.org/10.1007/s002310050137>
- Venkatachalappa M, Do Younghae Sankar M (2011). Effect of magnetic field on the heat and mass transfer in a vertical annulus. *Int. J. Eng. Sci.* 49:262–278. <http://dx.doi.org/10.1016/j.ijengsci.2010.12.002>
- Kefeng Shi, Wen-Qiang Lu (2006). Time evolution of double-diffusive convection in a vertical cylinder with radial temperature and axial solutal gradients. *Int. J. Heat. Mass Transfer* 49:995-1003. <http://dx.doi.org/10.1016/j.ijheatmasstransfer.2005.0.009>
- Takhar HS, Chamkha AJ, Nath G (2003). Unsteady mixed convection flow from a rotating vertical cone with a magnetic field, *Heat Mass Transfer* 39:297–304. <http://dx.doi.org/10.1007/s00231-002-0400-1>
- Teamah MA (2007). Numerical simulation of double diffusive laminar mixed convection in a horizontal annulus with hot, solutal and rotating inner cylinder. *Int. J. Thermal Sci.* 46:637–648. <http://dx.doi.org/10.1016/j.ijthermalsci.2006.09.002>.



International Journal of Physical Sciences

Related Journals Published by Academic Journals

- *African Journal of Pure and Applied Chemistry*
- *Journal of Internet and Information Systems*
- *Journal of Geology and Mining Research*
- *Journal of Oceanography and Marine Science*
- *Journal of Environmental Chemistry and Ecotoxicology*
- *Journal of Petroleum Technology and Alternative Fuels*

academicJournals